THE UNIVERSITY OF CHICAGO

CORTICOCORTICAL CONNECTIONS BETWEEN THE PRIMARY MOTOR AND SOMATOSENSORY CORTICES IN THE MACAQUE

A DISSERTATION SUBMITTED TO

THE FACULTY OF THE DIVISION OF THE BIOLOGICAL SCIENCES

AND THE PRITZKER SCHOOL OF MEDICINE

IN CANDIDACY FOR THE DEGREE OF

DOCTOR OF PHILOSOPHY

COMMITTEE ON COMPUTATIONAL NEUROSCIENCE

BY

SANGWOOK LEE

CHICAGO, ILLINOIS

MARCH 2019

To my advisor Nicho, the best mentor I have encountered.

For my parents, who supported me tirelessly in spite of great distance with endless love.

Most importantly, to my wife Latisha

and my child Liam

without whom I would have not understood endless love

ACKNOWLEDGEMENTS

Advisor

Nicholas Hatopoulos

Thesis Committee

Sliman Bensmaia

Leslie Kay

Yali Amit

Current and past Hatsopoulos lab

Alex Rajan

Caleb Sponheim

Carrie Anne Balcer

Dalton Moore

Fritzie Arce-McShane

Jeff Walker

Kazutaka Takahashi

Karthikeyan Balasubramanian

Marina Sundiang

Rebecca Junod

Vassilis Papadourakis

Wei Liang

Current and past Bensmaia lab

Elizaveta Okorokova

Gregg Tabot

James Goodman

Jeremy Winberry

TABLE OF CONTENTS

LIST OF FIGURES

LIST OF TABLES

Abstract

The goal of this thesis is to investigate the functional communication between primary motor (M1) and somatosensory (S1) cortices during the ethologically relevant behavior of hand grasping. Performing motor behaviors in our normal life requires the interplay between complex motor control and precisely timed somatosensory feedback. While many anatomical studies have shown cortico-cortical connections between M1 and S1, how somatosensory signals, in particular proprioception, functionally interact with motor area to guide natural hand movements is yet to be discovered. We sought to test the hypothesis that sites in M1 and S1 that shared similar somatotopic representations were more likely to be connected than paired sites that were somatotopically dissimilar.

We used a multi-camera motion capture system to track the kinematics of reflective markers placed on the hand and arm of the monkey, from which we reconstructed joint kinematics. High-density multi-electrode arrays were implanted in non-human primates to record neural signal from both M1 and S1 simultaneously while the monkeys engaged in a trained grasp task. Multivariate generalized linear modeling (GLM) was used to characterize the functional connectivity between signals recorded from different electrode channels. To provide more causal evidence for these interactions, intracortical microstimulation (ICMS) was used to infer the short-latency connectivity between M1 and S1 sites. This technique was applied to investigate cortical dynamic connectivity and the causal relations between local cortical networks.

Using both statistical and stimulation techniques, we found evidence for our hypothesis that sites in M1 and S1 that had similar receptive/projections fields were more likely to be functionally connected. Such connections may facilitate the synergistic coordination of movement with sensation.

Chapter 1: Introduction

One of the most important organs in our body is the hand. We interact with our surroundings using our hands, and advanced tool use with the hands has played an important role during primate evolution. In particular, the hand is an excellent tool for grasping a variety of different objects. It has allowed primate species to perform primitive actions such as foraging for food as well as more complex actions, including haptic exploration of objects (i.e. stereognosis) and tool use. The evolution of intricate finger movements has led to a unique expansion of the repertoire of possible hand conformations and movements, which suggests complex neural dynamics in hand sensorimotor control. In the context of food-related manipulation, it has been shown in primates that complex object manipulation using the hands is closely related to brain development, size, and relevant ecological aspects (Heldstab, 2016). Indeed, with exceptional brain-to-body mass ratio (and presumably, more complex sensorimotor system) and unusually long thumb, humans are able to perform more complex tool use than any primate species. Little is known, however, about the functional interactions between the primary somatosensory (S1) and motor (M1) cortices in the context of generating or modulating the hand movement. The sensory signals processed from S1 (i.e. cutaneous and proprioception) and the motor commands generated in M1 are crucial for accurate motor control and appropriate force application, as indicated by the severe effect of lesions in either M1 or S1 on hand movements (Schabrun et al. 2008; Ghez et al. 1995).

The goal of this study is to investigate the cortical communication structures between M1 and S1 during a natural hand grasping. Hand grasping is an ethologically relevant behavior that displays a high level of versatility depending on the physical properties of the object to be grasped and the structure of grasper's hand. Therefore, hand grasping has been widely used to investigate

the neural characteristics of hand motor control, although the experimental setting has been somewhat constrained and less natural. In an attempt to reduce these constraints, a multi-camera motion capture system was used to reconstruct the hand joint kinematics and chronically implanted high-density multi-electrode array captured the neural signals of M1 and S1 during the task. Collected data were analyzed to examine how neural signals from M1 and S1 interact with each other during the preshaping of the hand prior to object contact: that is, how different conformations of the spatiotemporal hand status characterizes (or is characterized by) corticocortical interaction of M1 and S1. By measuring the occurrence and directionality of functional connectivity and the sign and the strength of causal interactions between M1 and S1, we provide evidence for the hypothesis that these interactions are more prevalent between sites that share similar receptive and projection fields.

Several anatomical studies using anterograde and retrograde tracing methods as well as electrophysiological studies have investigated the connectivity between M1 and S1 and their projections to other brain areas and to the spinal cord. Most of those studies have focused on the geometry of connectivity structure and static projections, regardless of the temporal dynamics of the connections. In the second part of the introduction, I will briefly describe the studies that discovered the connections between cortical areas via either direct connections (corticocortical) or indirect connections (corticothalamocortical) in terms of sensorimotor transformation.

Somatosensory cortex (S1)

Somatosensation provides an important source of information for movement intention and guidance. Two well-known sensory modalities processed from S1 are tactile and proprioceptive sensations. They are originated from the periphery and are conveyed by muscle spindles

(proprioception, Houk et al., 1981), Golgi tendon organs (proprioception, Crago et al., 1982), joint receptors (tactile and proprioception, Ferrell et al., 1987), and cutaneous receptors (tactile, Edin, 2001). Individual or combined signals ultimately converge onto neurons in S1 in the postcentral gyrus of the parietal lobe. When we touch an object or move the fingers, it is believed that our perception depends on the activation of neurons in S1.

Sub-region of S1 S1 comprises four anatomically and functionally distinctive areas in which the above signals are processed. From the posterior to anterior directions, Brodmann's area 2 is located on the postcentral gyrus, area 1 is located anterior to area 2 hugging the posterior convexity of the central sulcus (CS), area 3b is located within the posterior bank of the CS and can extend close to the fundus of the CS, and finally, area 3a is buried in the fundus of CS and in some cases, it extends into the lower part of the anterior bank of the CS. Exact locations of sub-areas of S1 vary across the medial-lateral axis of the CS and across different animals even in the same species. These areas are reciprocally interconnected and process somatosensory signal serially and in parallel.

According to the hierarchical view of cortical organization, areas 3a and 3b are considered as "lower" areas and areas 1 and 2 are considered as "higher" areas. This is due to the fact that (1) areas 3b and 3a neurons possess smaller receptive fields than areas 1 and 2 neurons (Sur et al., 1985), (2) following the onset of a somatosensory stimulus responses in areas 3b and 3a tend to precede responses in areas 1 and 2 (Wolpaw, 1979), and (3) areas 3a and 3b receive direct inputs from thalamus, whereas areas 1 and 2 mostly get strong inputs from areas 3a and 3b, respectively (Cusick et al., 1985).

Responses of neurons in S1 during grasping provide important information for successful and delicate motor control. Specifically, joint, muscle spindle, and cutaneous information are

provided (Klatzky et al., 1993; Prud'homme et al., 1994; Krubitzer and Disbrow, 2008). The classical model of cortical somatosensory processing posits that the main function of neurons in area 3a, process proprioception, area 2 process both proprioceptive and cutaneous information whereas neurons in areas 3b and 1 process only cutaneous information. Using cutaneous stimulation (light touching, air puff, brushing or pressing the surface of the skin) and electrophysiological recordings, the Kaas group first mapped the macaque body representation of the neurons in S1 (specifically, in areas 3b and 1; Nelson et al., 1980). In S1, there is a contralateral body representation of the leg, trunk, proximal arm, hand, face, and mouth in the medial to lateral direction. An important finding of this study is that body representation of 3b and 1 is consistent (the term "mirror-images" is used in their study) with each other. The Krubitzer group further extended their work to area 3a (Krubitzer et al., 2004) in various primates and found the somatotopic organization of S1 is indeed consistent with each other, although the digit representations in area 3a are somewhat overlapping and less distinct than those in 3b, 1, and 2.

The neural map of the body in the brain does not duplicate exactly the spatial topography of the skin. Instead, it contains disproportionately larger areas devoted to the hand, foot, and mouth and relatively smaller areas devoted to more proximal body parts. Such cortical magnification suggests that greater numbers of neurons are necessary to process information received these body parts. In particular, evolution has shaped the primate's sensory cortical magnification of the hand for dexterous use of the fingers and tool use (Mountcastle, 2005). Such cortical magnification is also observed in the primary motor cortex (M1), containing the largest areas devoted for the hand and mouth representations.

Cortical pathways for visually guided hand grasping

Voluntary movement is expressed after subject's internal intention (the goal) is carried out by sensory information and the subject's internal cognitive states. To achieve the goal, our brain has to process a series of intermediate goals, such as interpreting inflowing information about the external world from sensory areas, creating an internal model to achieve the goal, planning the movement, and finally, executing the movement. No single area of neocortex is capable of processing all these steps and thus, different brain areas are sequentially and simultaneously activated to serve the functions and the goal.

Let us consider the action of catching a flying ball. Such a seemingly simple action requires a series of activations of sensory systems and precisely timed motor planning and executions. To perform a successful grasp, first, our brain has to estimate the future location of the ball based on the given visual information about ball's speed and direction. On top of that, visual information about the ball's physical properties, such as its shape and texture, would have to be encoded to plan the conformation of the hand for grasping. Moreover, the information about subject's current state of the arm (and hands) is also provided by somatosensory cortex and is integrated with the visual representations of the object in the parietal cortex. The parietal cortex then transforms the integrated multimodal sensory information into an internal model that can be applied to the goal-directed voluntary behavior. Planning of the reach-to-grasp occurs in this stage of the process. Motor planning is elaborated by premotor cortex from which motor execution is performed by the primary motor cortex. Carefully organized spatiotemporal muscle activation signals are sent to the spinal cord to activate appropriate upper limb muscles to accomplish the ultimate goal of grasping.

Posterior parietal cortex

The posterior parietal cortex plays a major role in the generation of goal directed movement. This is the area of the brain where the multimodal sensory information emerges, such as visual (Felleman and Van Essen, 1991; Maunsell and Van Essen, 1983; Ungerleider and Desimone, 1986), somatosensory (Jones and Powell, 1970; Pandya and Kuypers, 1969; Selzer and Pandya, 1980), and auditory (Divac et al. 1977; Pandya and Kyupers, 1969). Not only that, its function further serves the planning of the movement (Snyder et al. 1997) and attentional modulation (Quraishi et al. 2007). Since the early studies on the neural activity of parietal cortex (Mountcastle et al. 1975), researchers have highlighted the emergence of sensory information in the parietal cortex in the context of visually guided behavior. Due to the multifunctional nature of parietal area, it is further subdivided into several different specialized areas in terms of their functions and anatomical connections to other "lower-order" regions, in the view that information is processed in a hierarchical manner (Iwamura, 1998).

Somatosensory inputs to the parietal area The classic concept of hierarchical processing in the brain posits that lesioning "higher" order areas do not result in deficits in function of "lower" order areas. In this sense, posterior parietal cortex (PPC) has long been considered to be a higher order area than S1 as Peele and colleagues (Peele and Talmage, 1944) found that acute ablation of area 5 didn't result in the loss of nociception and tactile sensation in monkey. An anatomical study (Jones et al. 1970) further confirmed this hierarchy structure by finding one-way corticocortical connections from area 2 and 1 (higher order area of S1) to area 5. When they performed anterograde injections in the upper limb representations of areas 2 and 1 in the monkey, they found transported labeling in area 5, whereas the opposite didn't result in labeling in areas 2 and 1.

Somatosensory information is provided to PPC not only via direct corticocortical connections from S1, but also via a thalamocortical route. Padberg and colleagues (Padberg et al., 2009) used retrograde tracing techniques combined with electrophysiological recordings to trace the thalamocortical connections between thalamus and areas 5 as well as areas 3a, 3b, 1, 2, and 5. The tracers were injected into the hand representation of these areas and labels were confirmed mostly in the ventral posterior complex of thalamus. In this study, they found that area 5 receives sparse projections from ventral posterior (VP), ventral posterior inferior (VPi), and posterior division of the ventral lateral (VLp) nucleus and dense projections from ventral posterior superior (VPs), anterior pulvinar (PIa), and lateral posterior (LP) nucleus. Proprioceptive input via VPs and cutaneous input via VPi and PIa are necessary for generating an internal representation of the body.

Ventral intraparietal area (VIP) In the context of generation of visually guided hand grasping behavior, VIP (ventral intraparietal; located in about the middle third of the fundus of the intraparietal sulcus) is a major sub-area that integrates visual and somatosensory signals. Duhamel and his colleagues (Duhamel et al. 1998) found that neurons in macaque VIP can be divided into two groups; unimodal (only visual sensitive) and bimodal (both visual and tactile sensitive). 85% of bimodal neurons' visual and tactile RFs are aligned in a congruent manner such that the locations of their tactile RFs on the body match the locations of the peripersonal visual RFs near the corresponding body part. Further investigations of the VIP neurons showed modulations to head and eye movement as well as object movement in peripersonal space (Bremmer et al. 2002, Klam and Graf, 2003). Selective modulation of VIP neurons for object movement in peripersonal space suggests their involvement in their generation of either or both reach and grasp behaviors.

Anterior intraparietal area (AIP) Much like other sub-regions of the intraparietal area, neurons in AIP (located in the rostral/anterior part of the lateral wall of the intraparietal sulcus) exhibit multimodal response properties. In particular, neurons in AIP area display selectivity for visually presented objects to be grasped. These neurons differentially modulate for different grasp types such as precision grip, whole hand grip, and well as other more complex multi-digit grasping (Taira et al., 1990, Sakata et al., 1995). These neurons possess visual receptive fields whose size vary widely across AIP and are retinotopically organized in the subject's visual hemifield reference frame (Romero and Janssen, 2016). Due to their strong selectivity for object shape and other visual properties, neurons in AIP is of special interest for study of grasping behavior. Interestingly, however, only one lesion study has found that inactivation of AIP results in disturbances in grasping (prehension) (Gallese et al., 1994).

The functional significance of neurons in AIP in grasping movement occurs in the early stages of movement planning. AIP neurons fire maximally before the hand movement onset time and object contact (Gallese et al., 1994). Several decoding studies have investigated AIP neurons' role in motor planning (Lehmann and Scherberger, 2015 and Schaffelhofer et al., 2015). In summary, AIP arguably plays indispensable role in the sensorimotor transformation of the grasping behavior and it is situated at an early stage of visuo-motor planning and execution.

Premotor cortex

Premotor cortex (PM) is situated immediately anterior of the primary motor cortex (M1) in the frontal lobe of primate brain. Neurons in PM are thought to be mainly involved in transforming the intention of the movement to the proper motor act. Although many studies have focused on its function in motor preparation, recent study also pointed out that PM neurons are

involved in the use of recent and long-term sensory memory to decide, execute, and evaluate the outcomes of decisions (Pardo-Vazquez et al., 2011).

The intention to grasp an object, along with the visual and somatosensory information, is transferred from parietal cortex to PM through parietofrontal cortical pathways. Traditionally, it is considered that hand grasping movement arises from the most anterior lateral part of PM near the lateral end of arcuate sulcus, called ventral premotor cortex (F5). This is supported by the fact that neurons in F5 are strongly modulated by distal upper limb (hand) muscle activity (Rizzolatti et al., 1988) and display selectivity for the physical properties of objects to be grasp, such as size, shape, and orientation (Murata et al., 2000).

Corticocortical connections between AIP and F5 As major components of the grasp network, F5 and AIP have strong corticocortical connections. Luppino and colleagues used the cell labeling method to find the reciprocal and direct connections between neurons in F5 and AIP of macaque (Luppino et al., 1999). Another anatomical tracing study further confirmed connection structure of AIP to other brain areas and found AIP is the main source of projections to F5 (Borra et al., 2007). The authors of above studies concluded that the connections between F5 and AIP are the main routes of the visuomotor transformations for grasping behavior. They share some similar neural properties with each other as mentioned above. Temporary lesioning (inactivation) of either AIP (Gallese at al., 1994) or F5 (Fogassi et al., 2001) results in deficits in anticipatory shaping of the hand during grasping. However, these two areas do exhibit some differences in functional properties. Most F5 neurons that respond to the hand manipulation of the object, show different neural modulations when the subject is asked to manipulate the same object in the dark room (Murata et al., 1997). In addition, many neurons in F5 represents the goal of action rather than the

specific effectors used to perform the motor action. For example, many neurons in F5 fire when grasping is executed with effectors as different as the right or left hand, and even the mouth. Taking together, the functional role of neurons in F5 for visually guided grasping behavior is to elaborate the goal of actions, select a grasp type based on the object's intrinsic properties, and transfer this signal to M1 where more specified and detailed movement generation occurs.

Primary motor cortex (M1)

M1 is considered the major final output stage of movement generation in the cerebral cortex. Neurons in M1 translate the selected motor plan into motor commands that are relayed down the spinal cord. These translations include (1) recognizing the extrinsic kinematic features (i.e. the location of the object), (2) calculating the necessary intrinsic kinematic features (i.e. current state of the effectors), and (3) applying appropriate kinetics for the dynamic movements. Several sub-populations of neurons in M1 are known to perform these tasks to generate goal-directed movement (Jessell et al., 2000).

Since Dr. Jackson's proposal in the mid-19th century that the cortex immediately anterior to the central sulcus is responsible for generation of movement, numerous studies have been devoted to answer the question of how neurons in M1 work to generate the voluntary movement. A breakthrough cortical stimulation experiment done by Gustav Fritsch and Eduard Hitzig (1870), shed a light on the somatotopic organization of M1. Woolsey (1949, mammal subject) and Penfield (1937, human subject) independently confirmed a topographic organization of M1, using more localized stimulation (intra-cortical microstimulation, or ICMS) technique. As seen in primary sensory cortices, these studies demonstrated that the sizes of cortical areas stimulated to evoke movements of different body parts were disproportionally represented. Instead, the body part that

requires fine muscle control or various conformations, such as hand or mouth, dominated a huge portion of the precentral gyrus.

Projection to the spinal cord M1 as well as other cortical motor regions (premotor, supplementary motor, and parietal cortices) make projections to subcortical areas and to the spinal cord via the corticospinal tract. In most mammals, corticospinal neurons in layer V of M1 project to interneurons in the intermediate region of the spinal cord. In certain primates (old world monkeys, great apes, and humans), however, there is special pathway from M1 to the spinal cord, called the corticomotoneuronal (CM) pathway where layer V neurons make direct and monosynaptic connections to motor neurons in the ventral horn of the spinal cord. The Strick group found that a single CM cell forms branches that connect to many motorneurons such that it can coactivate a set of muscles and generate functional synergies (Rathelot and Strick, 2009). The widespread distribution of CM cells of a single muscle and extensive intermingling of CM cells is thought to create a broad range of functional synergies.

Topographic organization of M1 The ICMS technique has been used to map out the projection fields (PF) of sites across M1 (Kwan et al., 1978; Nudo et al., 1992; Stepniewska et al., 1993; Park et al., 2001). Their studies are mostly restricted to mapping the spatial organization of muscle representations in primate M1, especially of the upper limb. Park and his colleagues used a combination of ICMS and electromyography (EMG) to generate stimulation-triggered average EMG profiles of various muscles of the upper limb. As others had found, they found that the distal limb muscle representations (i.e. digit, hand, wrist) is concentrated in a central core of the precentral gyrus. This area is surrounded by an area that triggered both distal and proximal muscle

(i.e. arm and shoulder) representations and is even further surrounded by an area with only proximal muscle representations. The finding of a mixing zone of distal and proximal muscle representations corresponds to many other studies that recognized that nearby sites in motor cortex could represent or evoke very different muscles and joints (Donoghue et al., 1992; Schieber and Hibbard; Sanes et al., 1995).

Rostral and caudal M1 Further investigation using retrograde trans-synaptic, tracing method revealed the presence of rostro-caudal spatial organization within M1. The Strick group (Rathelot and Strick, 2009) injected rabies virus into one of three forelimb muscles of macaque: abductor pollicis longus (one of the extrinsic muscles of the arm/wrist), adductor pollicis (adductor of the thumb), and extensor digitorum muscle (posterior forearm muscle). They investigated the location of cell bodies of CM neurons in M1 that make direct projections to motor neurons. They found that CM cells were located predominantly within the anterior bank of the central sulcus and very few of these cells were on the precentral gyrus. Strick group's study has led to the conclusion that M1 can be subdivided into two areas; In the rostral part of M1 (rM1), there are fewer number of CM cells and many neurons respond to cutaneous sensory input. In the caudal part of M1 (cM1), there are many CM cells, and many neurons respond to deep somatosensory input.

What do neurons in M1 encode? Although it may seem obvious that neurons in M1 are nothing more than "muscle activators", their exact function in generation of movement is not straightforward. The question of what features of movement do neurons in M1 represent has been unresolved and the subject of debate among many researchers for many decades. Evart (Evart, 1968) is the first who recorded neural activity of M1 while awake. behaving monkeys performed

single-joint, voluntary movements. Monkeys engaged in a lifting task using pulleys and weights while Evart recorded single units from M1 hand and wrist area. He found that the many neurons in M1 increased their firing rate during movements when the load opposed the movement but decreased when the load assisted it. Evarts' studies led him to conclude that M1 neurons encode muscular force (i.e. kinetics).

Georgopoulos pioneered the study of encoding of M1 neurons using multi-joint movements (Georgopoulos et al., 1982) and demonstrated that the direction of the movement (i.e. kinematics) is an encoded feature of M1 neurons and that activities from populations of neurons can be linearly combined to decode the direction of upcoming movement (referred to as population vector decoding).

These early studies inspired many research groups to investigate a variety of different movement parameters encoded in M1. Movement direction (Georgopoulos et al., 1984), velocity (Paninski et al., 2004; Moran and Schwartz, 1999), acceleration (Stark et al., 2007), and force and torque (Evarts, 1968; Kalaska et al., 1989; Taira et al., 1996; Cabel et al., 2001) have been considered as movement features that drive activity of M1 neurons.

Under the assumption that a linear model can effectively capture an individual neuron's feature selectivity, it is possible to construct a multiple linear regression framework to investigate single neuron's firing property, using a number of movement features. For example, we can model single M1 neuron's firing rate as follows:

$$\vec{r}(t) = G(\vec{a} \cdot \vec{P}(t+\tau) + \vec{b} \cdot \vec{V}(t+\tau) + \vec{c} \cdot \vec{A}(t+\tau) + \vec{d} \cdot \vec{F}(t+\tau) + \vec{h}) \qquad (1)$$

where P is position, V is velocity, A is acceleration, F is force (or torque) of an effector (in this case, I am assuming the arm), h is the baseline firing rate, and τ is the time lag between the measured movement feature and measured neuronal response. G is a special nonlinear term applied

to compensate for the fact that the firing rate must span from 0 to any positive number. Popular choice includes any family of exponential functions (softplus, or logistic function). The goal of such a model framework is to infer model parameters and to investigate to which features neurons are the most responsive. Then, the typical task to investigate neuron's feature selectivity under such a linear-nonlinear cascade model framework would be expressed as

$$\mathcal{L} = \underset{a,b,c,d,h}{\arg min} \, ||r(t) - \bar{r}(t)||_2^2 \qquad (2)$$

where r(t) is a true firing rate in time. The difficulty of such optimization problem depends on the choice of nonlinearity, the number of movement features in the equation, and/or the dependency structure of the selected features. With this approach, it is possible to measure the importance of features to the neuron's firing. A few more additions to the model have helped to improve the model predictability. The context dependency nature of M1 neurons (i.e. neural plasticity) is ignored in the above model framework (i.e. feature parameters may vary in time). In fact, many researchers pointed out that neuron's preference for certain features, such as direction, can change during the task (Mason et al., 1998; Sergio and Kalasak, 1998; Churchland and Shenoy, 2007), indicating it is necessary to take temporal dynamics of feature selectivity into account. Our group found that implementing above points into the general linear-nonlinear-Poisson spike generator model framework significantly improves M1 single neuron model performance (Hatsopoulos et al., 2007). Specifically, the advanced model included

- Multiple time lags and leads between neural spiking and arm velocity component.
- Average speed and position terms.
- Prediction is on the probability of the firing rate in a given time bin, not actual firing rate, considering Poisson spike generation (point process).

More recently, Saleh (Saleh et al., 2012) applied the same model framework M1 neurons in monkeys performing a grasping task. Their work included spike history terms to incorporate non-Poisson history dependencies that affect upcoming spiking probability (e.g. refractory period, oscillations, or calcium potassium dependent afterhypolarization effect), which provided a more biologically plausible model. In addition to their finding that temporally extensive kinematics trajectories yielded significantly higher predictive performance than simple single lag models, neurons tended to encode feature velocities over positions and multiple kinematic features were encoded in single neurons of M1.

Local field potential signal and its source in a cortical circuit

Information about single unit neuronal activity can be extracted by using extracellular recording technique, and it has been powerful tool for learning nature of the cortical activity. Neuron's electrical activity, or electrical potential, is measured by a inserting sharp electrode into brain tissue and in close vicinity to the neuron cell bodies and neuropil. The collective electrical activity of the local population of neurons in a given location of brain tissue generates and contributes to the measurement of a potential. The recorded extracellular potential is filtered with a high frequency filter (greater than 500 Hz) to obtain action potentials from nearby cells, and with a low frequency filter (less than 500 Hz) to investigate aggregate potentials from local neuronal populations, referred to as the local field potentials (LFP). The information that the LFP provides is difficult to interpret and localize its sources, as it is summed activity of local neurons spanning a hundred of micrometers (Kajikawa et al., 2011).

What are the possible sources of the local field potential? In order to interpret what we obtain from an extracellular recording, it is important to know how this signal is created. Assuming

that conductivity in the brain is purely ohmic, the synaptic activity of local neurons contributes to the extracellular potentials as hundreds to tens of thousands of synapses of each neuron result in inflow and outflow of positive and negative ions. The positive current flow from the intracellular space to extracellular space is called a *source* and the opposite is called a *sink*. The spatial separation of sink and source gives rise to an electrical dipole within each neuron. Depending on the location of the current flow with respect to the recording site, it creates the electric potential which contributes to the realization of LFP. The geometry of neural dendrites determines whether a measured LFP is generated from the dipoles within individual neurons. If local neuronal populations display randomly oriented dendritic trees with a symmetric closed field geometry, individual dipoles will cancel each other resulting very little or no contributions to the LFP. Cortical pyramidal neurons whose apical dendrites are all positioned parallel to each other's (normal to the cortical surface) exhibit an open field geometry. When these neurons are synchronously activated, their dipoles are aligned and create more robust contributions to the LFP signal. Other possible contributors to the LFP include i) the intrinsic resonance of membrane structure of neurons (Silva et al., 1991), ii) neuron and glia electrical interactions (Poskanzer and Yuste, 2011), iii) dendritic Ca^{2+} spikes (Hirsch et al., 1995), and iv) more direct electrical interactions between neurons via gap junctions (Traub et al., 2004).

Identifying the location of current flow across the membrane is important because it is directly correlated with fluctuation of measured low frequency potentials (or LFP). Theoretically, the portion of the extracellular potential, $p_0(t)$, measured at position r because of a membrane current $I_0(t)$ at position r_0 is

$$p_0(r,t) = \frac{1}{4\pi\sigma}\frac{I_0(t)}{|r - r_0|}$$

, where σ is the extracellular conductivity which is assumed to be constant but may vary across different brain areas or differes between gray and white matters (white matter has a lower conductivity than cortical grey matter). Thus, a total potential is formulated as a sum of transmembrane currents divided by distance of each source, or $p(r,t) = \frac{1}{4\pi\sigma}\sum_{n=1}^{N}\frac{I_n(t)}{|r-r_n|}$ (1). A net current flow through a point (or the location of transmembrane called current source density, C(r)) can be computed by Ohm's law, the definition of p(r,t), and the fact that C(r) = -σΔp, where Δ represents the spatial second derivative. Traditionally, CSD analysis is done using LFPs recorded by laminar (linear) multi-electrode arrays with a constant inter-channel distance inserted perpendicularly to the cortical surface. CSD has been widely used to identify the origin of the current with given information about cortical circuit structure (Bragin et al., 1995, Rainer and Gregor, 2015). CSD is more straightforward to relate to neural activity than the LFP itself, though the combination of CSD and other measurement methods may be used to identify the dynamics of measured potential (Buzsáki et al., 2012), and thus CSD analysis has become a standard tool for analysis of the extracellular potentials.

Connections between M1 and other areas

One of the earliest and most important goals of neuroscience study has been to investigate the functional properties of neurons in a target region and the contribution of other pathways to neurons in that target area. Therefore, studying cortical interactions is an important goal for neocortical research as most of cerebral cortical areas receive projections from many cortical and subcortical areas. In this sense, studying cortical function via a single afferent (efferent) pathway would give us only one part of the whole story and limit our understanding of how the brain functions.

The motor cortex is the one of the earliest studied cortical areas from a functional point of view. However, due to limitation in methodology and complexity of experimental design, our knowledge about the functional interactions between M1 and other areas is limited. However, classic experiments have confirmed that M1 is reciprocally interconnected with S1 and receives projections from ventral anterior and ventral lateral nuclei of thalamus.

Thalamocortical somatosensory inputs to M1 Neurons in M1 of the vertebrate brain are reciprocally connected with many other brain areas and these connections process fast feedback control (Pruszynski et al., 2011). Part of this sensory feedback signal is thought to be sent to the S1 as lesion studies have provided compelling evidence of the effect of S1 lesions in the motor control. S1 lesions result in unstable finger movements and poorly organized grasp behaviors (Sainburg et al., 1995). Despite these deficits in fine motor control, these lesions do not lead to the complete inability to perceive somatosensory input, suggesting that M1 receives direct somatosensory input from the thalamus.

All somatosensory afferent signals originate from somatosensory peripheral nerves and are transmitted to the higher centers of the brain through the spinal cord and are called ascending somatosensory pathways. There are several distinct somatosensory pathways: proprioceptive, tactile and nociceptive (pain and thermal) information which travel through the dorsal column/medial lemniscal system and spinothalamic tract. The cerebellum receives somatosensory information through the spinocerebellar tract which in turn projects to the somatosensory cortex through the thalamus. The thalamus plays an indispensable role in most of the functions of the cerebral cortex such as relaying sensory and motor signals to the corresponding areas (Siegelbaum et al. 2000). Ventral anterior and ventral lateral nuclei of the thalamus are important for motor

control and carry information from the basal ganglia and cerebellum to the motor cortex. The part of the ventral posterior lateral nucleus, ventralis posterior lateralis pars caudalis (VPLc), conveys somatosensory information to the neocortex. In addition to relaying sensory and motor signals to the neocortex, the thalamus also may play a role in cognitive function by communicating with prefrontal cortex and regulates the activity of other nuclei through GABAergic inhibitory neurons. Therefore, the thalamus is not just a passive relay station but a complex brain region where substantial information processing is possible. Retrograde labeling (Dinopoulos, 1994) and electrophysiological (Lenz et al., 1994) studies indicate the existence of thalamothalamic connections in subdivisions of the ventral thalamus area, although the function of those connections is not yet known.

Subdivision of the ventral thalamic groups such as the ventral anterior and ventral lateral nuclei may provide partial information about somatosensory signals provided the existence of internal connection within the ventral thalamic group (i.e. connection between ventral lateral and ventral posterior) (Holtzman, 2012). Also, the signals projected from cerebellum to ventralis posterior lateralis pars oralis (VPLo) may consist of somatosensory information originating from the spinocerebellar tract.

Corticocortical connections between F5 and M1 Of particular interest to grasping behavior, neurons in F5 (lateral portion of PMv) are active during grasping and possess a direct connection with M1. This connection, highlighted by Jeannerod (Jeannerod et al., 1995), represents a significant route of the grasping network. Retrograde tracing method (Muakkassa and Strick, 1979; Godschalk et al., 1984), transcranial magnetic stimulation (TMS) study (Bäumer et al., 2009), and ICMS (Kraskov et al., 2011) confirmed non-random, reciprocal, and task related neuronal

connections between F5 and hand area of M1. In particular, the Brochier group (Kraskov et al., 2011) recently conducted ICMS study to investigate the short-latency corticocortical connections between F5 and the M1 hand region while monkeys were actively engaging in a grasping task. This study confirmed short-latency excitatory connections with weak currents while progressively more inhibitory connections dominate as the amplitude of stimulating current increases.

Corticocortical connections between M1 and S1 Direct and reciprocal connections between M1 and S1 are known to exist in many animal species, such as the rodent (Farkas et al., 1999; Sato and Svoboda, 2010; Rocco-Donovan et al., 2011; Petrof et al., 2015; Kinnischtzke et al., 2016), felines (Blum et al., 1968; Thompson et al. 1970; Asanuma et al. 1968; Zarzecki et al., 1978; Asanuma et al., 1982; Herman et al., 1985) and macaque (Jones et al., 1978). The most direct way to infer anatomical corticocortical connections between M1 and S1 is using tract tracers that Jones and colleagues demonstrated (Jones et al., 1978). They used two types of injections: localized injections of isotope (autoradiographic) and broader injections of horseradish peroxidase (retrograde) to visualize cortical projections between areas 1,2,3 (S1),4 (M1), and 5. They focused the injection site on the forelimb area of M1 and S1, as well as area 5. They found that

- Area 3b is not connected to area 3a or area 4, but projects to area 1 and 2
- Area 1 is reciprocally connected with area 3a and 3b
- Area 2 is reciprocally connected with area 4 and 3a

From this study, they confirmed the close interplay between the motor cortex and sub-regions of the somatosensory cortex in which proprioception is mainly processed. Interestingly, they considered that there is a general topographic organization in the projection of one field of the

sensorimotor region to another, which suggests non-randomness of the connections in the sensorimotor area of macaque.

The functional significance of corticocortical connections (or even corticothalamocortical connections) between areas has been particularly well studied in the visual system (Cleland et al., 1971; Mciiwain, 1973, 1977; Tanaka, 1983; Ts'o et al., 1986; Hata et al., 1991; Salin et al., 1992). Salin and colleagues investigated the functional organization of corticocortical connections between area 18 (primary visual area, or called V1) and 17 (secondary visual area, or called V2) in cat, using a combination of electrophysiological recording and neuroanatomical tracing method. Although not ideal due to the fact that the retrograde tracing uptake zone is rather broad, they found a strong retinotropic organization of corticocortical connections between area 17 and 18; most units that have reciprocal connections between areas 17 and 18 share their RF locations in the visual field. A similar tendency also is observed in other RF properties of V1 and V2 cells (Roe and Ts'o, 1992). For example, in the color domain, color cell pairs with matched color specificities exhibit correlation peaks.

Corticocortical connections in terms of their functional specificities in the sensorimotor area was extensively examined by the Asanuma group beginning in the late 1960's in cats (Asanuma et al., 1968; Thompson et al., 1970, Asanuma et al., 1982; Herman et al., 1985). The early studies in anesthetized cat using a combination of ICMS and electromyograms (EMGs) techniques confirmed that many regions in pericruciate cortex (72%) project to a common motoneuron pool and receive cutaneous information from a localized skin region. Proprioceptive afferent also displayed the same tendency. The same group (Thompson et al., 1970) confirmed corticocortical connections between Ms1 and Sm1 (analogous to M1 and S1 in primate,

respectively) and are organized somatotopically. They found a short-latency ICMS responses from Sm1 to Ms1 sites that share a common RF region (front paw skin and joints).

In summary, anatomical connections between M1 and S1 exist across many animal species. However, their functional significance particularly in the primate species has not been studied. Moreover, no previous M1 and S1 corticocortical connectivity study has been done while the animal subject is performing motor task. Here, we propose the hypothesis that corticocortical interactions between M1 and S1 in macaque monkey are organized bidirectionally and somatotopically. The above studies (Asanuma et al., 1968; Thompson et al., 1970) support this hypothesis. We propose two experiment paradigms to test the above hypothesis.

We will use rhesus macaques to study how complex and natural hand movements are represented in M1 and examine the interplay between M1 with subdivisions of S1, especially in areas 3a and 2 in which proprioceptive responses are observed. In chapter 1, we will use the LFP signal collected from one site (either M1 or S1) and measure the correlation structure to the spiking activity sampled from another site (i.e. M1 LFP and S1 spiking and vice versa). Monkeys will be engaged in a precisely timed grasping task while hand joint kinematic data will be collected and analyzed along with neural data. The relationship between electrophysiological signals with joint kinematics will be analyzed to examine the similarity/dissimilarity of receptive and projections fields of pairs of M1 and S1 neurons. In chapter 2, we will infer causal interactions between M1 and S1 sites using ICMS. State-of-the-art multi-electrode arrays will enable us to simultaneously record and stimulate from multiple cortical sites. This study will be used to consider the directionality and sign of interactions between M1 and S1 in different epochs of a grasping task (i.e. pre-movement vs. after movement onset).

Subsequently, in the discussion section, we will discuss the finding of this thesis and possible future work to advance our understanding about the functional interactions in the sensorimotor system.

Chapter 2: Somatotopic organization of cortical interactions between the primary motor and somatosensory cortices in macaque

Abstract

Primary motor (M1) and somatosensory (S1) cortical area of primates are known to be anatomically interconnected. However, very little is known how proprioceptive signaling in S1 interacts with M1 to control naturalistic motor behavior such as grasping. By statistically analyzing spatiotemporal interactions between the spikes and the local field potentials (LFPs) recorded across the areas, we tested the hypothesis that M1 and S1 sites that share similar somatotopic response fields (RFs) of the hand would exhibit stronger functional connections than pairs with dissimilar RFs. Two macaques were trained to grasp over 30 different objects and multi-camera Vicon motion capture system tracked the kinematics of reflective markers placed on the hand and arm of the monkey from which we reconstructed the joint kinematics. We used high-density multi-electrode arrays to sample single unit activity and LFPs from rostral and caudal portions of M1 and area 3a and 2 of S1. Generalized linear model (GLM) was used to estimate the RFs of each neuron and to compute the significance of LFP component in predicting spiking activity, in addition to the hand joint kinematics. Our results show that there exists reciprocal functional interactions between M1 and S1 which are somatotopically organized: recording site pairs with shared RFs provide significantly more information about one another above and beyond what joint kinematics alone can explain.

Introduction

Grasping is a fundamental primate motor behavior that is critical for interactions with objects in the environment. The evolution of intricate finger movements has led to a unique expansion of the repertoire of possible hand conformations and movements, which suggests complex neural dynamics underlying hand sensorimotor control. Not only the primary motor (M1) and somatosensory area (S1), but also many other cortical areas are involved in the generation of visually guided hand grasping behavior. A recent model of the pathway for grasping behavior posits that somatosensory information provided to M1 is delivered indirectly either via thalamus or other multiple cortical areas, including anterior intraparietal (AIP) and ventral premotor area (PMv). Compelling evidence for the direct short-latency interactions between M1 and S1, however, has been suggested in anatomical tracing (Jones et al., 1978), intracortical microstimulation (ICMS) (Asanuma et al., 1968; Thompson et al., 1970; Asanuma et al., 1982; Herman et al., 1985), and optogenetic studies (Rocco-Donovan et al., 2011; Petrof et al., 2015; Kinnischtzke et al., 2016).

The functional significance of the cortical connections between M1 and S1 was investigated by Asanuma group in cats (Asanuma, 1968). Having established the fact that M1 and S1 are somatotopically organized, they hypothesized that neurons with similar receptive/projection fields response fields preferentially interact with each other, even across cortical areas. Indeed, in cats' motosensory area (analogous to primate's M1), the cutaneous receptive fields of neurons within a given efferent zone were most frequently found on a skin region that lay above the muscles comprising the efferent zone (Asanuma, 1968). Later, the same group further confirmed a topographical organization in the Sm1 (analogous to primate's S1) - Ms1 (analogous to primate's M1) corticocortical projections in cat. These previous studies investigated such interaction

structures in anesthetized animals with passive stimulations. What is unknown is whether such interaction structure in the sensorimotor cortex exists in the awake, behaving primate.

Here, we tested the hypothesis that the functional interactions between M1 and S1 in primate are somatotopically organized such that paired sites in the two areas that share similar response fields (RFs) are more likely to be functionally connected and exhibit stronger connectivity. We first mapped the RF (i.e. the receptive or projection field) of each neuron by using a generalized linear model (GLM) to predict its spiking response using the kinematics of the wrist and finger joints as covariates in the model. We then used the band-pass filtered local field potential (LFP) recorded on another site (i.e. a site not in the same cortical area), a proxy of local population activity on that site, as an additional covariate to the GLM model to determine whether the spiking response could be more accurately predicted. By comparing the model's performance with and without the LFP covariate, we measured the strength of the functional interaction between the single unit recorded in one cortical area and the local population activity recorded in another cortical area. In this way, we could systematically relate the strength of functional interactions with the pairs' RF structures. We found that reciprocal functional interactions between M1 and S1 which supported our hypothesis.

Materials and Method

Behavioral task: Two rhesus macaques (monkey J and B) were trained to grasp objects with their right hand. Each subject was trained to sit in a custom designed monkey chair with armrests on which subjects were trained to place their arms (Figure 1.1A). Light sensors were placed under the armrests and detected if the subject was correctly resting his arms. If the subject removed his

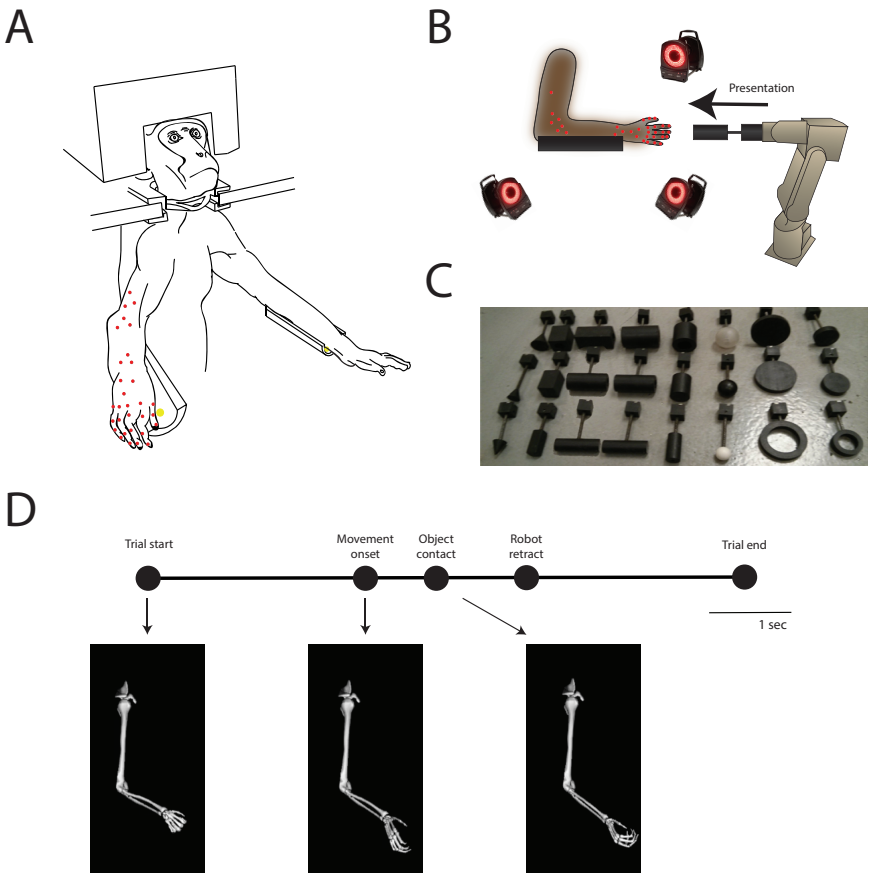

Figure 1. 1. Behavioral task setup

(A) The subject is trained to place his arms on the armrest. 31 reflective markers (red) were placed on subject's right hand and arm, from which we measured the position to reconstruct the joint kinematics. Light diodes (yellow) were placed on the armrest which detected if the subject is correctly resting his arm. (B) 14-Vicon camera system captured the position of reflective markers (red) while the object was delivered to the subject by robotic arm. (C) 24 different kinds of objects were used to create 35 distinctive combination of object presentations, varying its presenting orientation for subset of objects. (D) Task timeline. The trial started as the robot started to move the object towards the subject's hand. As the robot moved closer to the hand, the subject pre-shaped his hand to grasp the object. The subject was instructed to hold the object until the robot retracted it at which point the hand released the object.

arms from the armrests in any time point in a trial, it triggered an aborted trial signal. Once the monkey maintained a preparatory posture (resting both arms on the armrests), he was presented, on each trial, with an object by a robotic arm (Mitsubishi RV-1A-SI1, Tokyo, Japan) and grasped the object (Figure 1.1B). Objects were attached to the robotic arm with rare earth magnets,

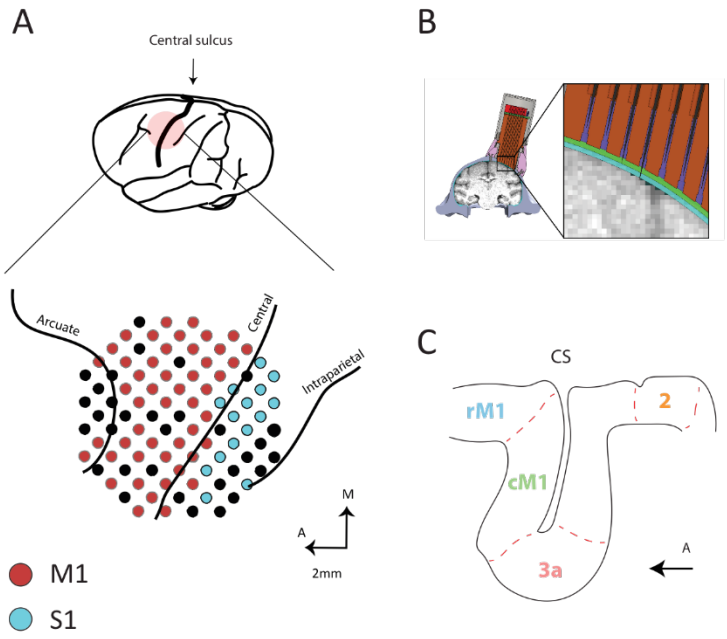

Figure 1. 2. Electrophysiological setup.
(A) Location of placement of Gray-matter microdrive system. (B) A view from anterior side. Individual electrode can be advanced and retracted up to 32 mm depth. (C) Drawing of parasagittal view of sensorimotor cortical areas, showing subregion of M1 (rM1 and cM1) and S1 (area 2 and 3a).

allowing them to be switched out quickly from trial to trial. A pseudorandom delay interval (0.5~1.5 sec) was applied between the initial grasp and the robotic arm retraction to its initial position (Figure 1.1D). Subjects were required to maintain a firm grasp and were rewarded for successful holding and detaching the object from the robotic arm. If, at any time point of a trial, the subject did not maintain contact with the armrest or detached the object prior to the retraction of the robotic arm (that is, detaching the object by pulling his arm), the trial was aborted. To elicit a variety of hand pre-shaping kinematics and different hand conformations for grasping, we used a set of geometric objects varying its shape, size, and orientation (Figure 1.1C). For example, as the size of object increased, the degree of abduction and extension of the fingers also increased. To the extent possible, the use of a large variety of objects served to minimize correlations between the movements of individual joints of the hand. Nine different object shapes were used in this study (block, cylinder, sphere, circle, ring, disk, point, cup, and cone). The block and cylinder were presented in 3 different orientations (vertical, horizontal, or pointing), and the ring and disk were presented in 2 different orientations (vertical or horizontal). Except for the point and cup shapes, all were presented in 3 different sizes (small, medium and large), making the total

number of possible distinct objects to be 35. On average, each subject completed 10 repeated trials of each object per session.

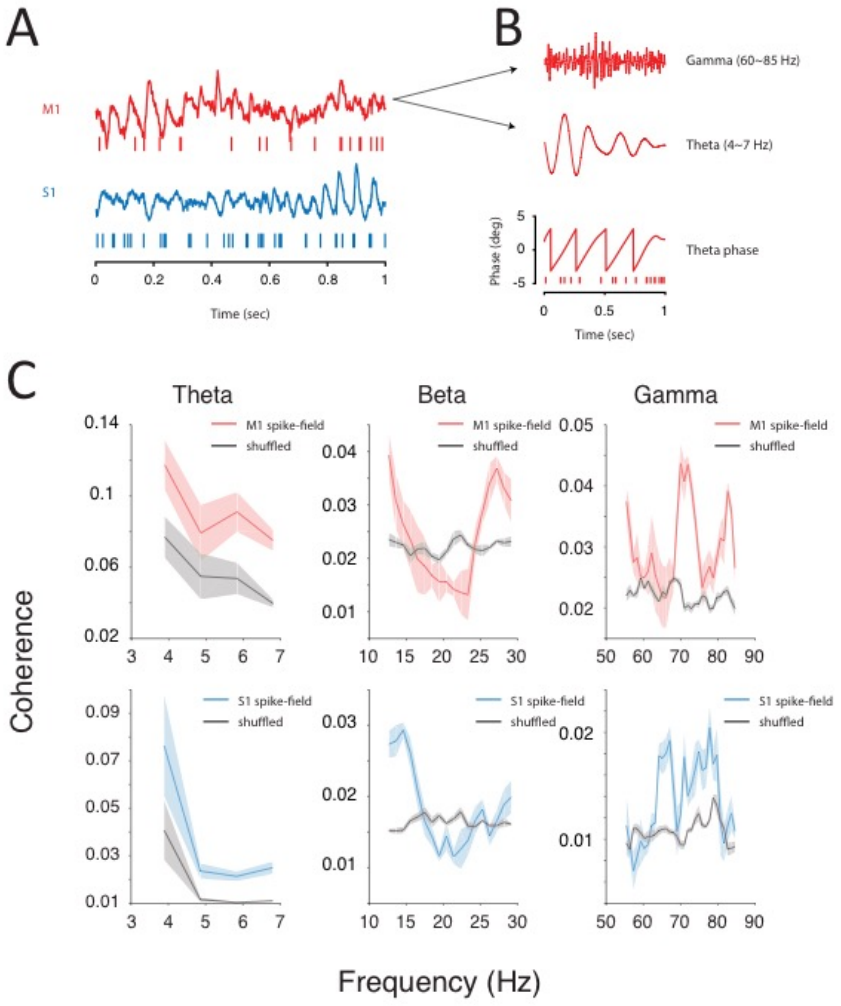

Figure 1. 3. Electrophysiological data
(A) Example local field potential (LFP) and spiking data from the same electrode (M1: red and S1: blue). (B) Gamma and theta band pass filtered LFP of an example data presented in (A). Phase of theta band LFP in time as well as spiking data. (C) Spike-field coherence of M1 (red) and S1 (blue). Spiking and LFP data are sampled in the same electrode to compute the coherence. Trial shuffled spike-field coherence is shown (black).

Motion tracking and inverse kinematics: Motion tracking was performed using a 14-camera Vicon Motion Tracking System (Vicon Motion Systems, Oxford, UK). The system tracked the three-dimensional positions of reflective markers (3 mm diameter) attached to the subject's dorsal hand and dorsolateral arm (Figure 1.1A). From these 3D coordinates, joint kinematics were reconstructed as function of time using a model of the primate forelimb in OpenSim (Delp et al., 2007) (Figure 1.1D). A total of 31 markers were used to compute joint angles in the arm and hand including: wrist pronation/supination, wrist flexion/extension, first digit carpal-metacarpal

(1 CMC) flexion/extension, 1 CMC abduction/adduction, 1 CMC pronation/supination, 4 CMC flexion/extension, 5 CMC flexion/extension, 5 CMC abduction/adduction, first digit metacarpal-phalangeal (1 MCP) flexion/extension, 1 MCP abduction/adduction, first digit inter-phalangeal (1 IP) flexion/extension, 2 MCP abduction/adduction, 2 MCP flexion/extension, 2 proximal-middle interphalangeal (PM) flexion/extension, 3 MCP abduction/adduction, 3 MCP flexion/extension, 3 PM flexion/extension, 4 MCP abduction/adduction, 4 MCP flexion/extension, 4 PM flexion/extension, 5 MCP abduction/adduction, 5 MCP flexion/extension, and 5 PM flexion/extension. The kinematic data were sampled at 100 Hz and bi-directionally filtered with a fourth-order Butterworth low-pass filter with 6 Hz cut off frequency. All data filtering and computations were done in MATLAB (The MathWorks, Inc., Natick, MA). The finger movement onset time was determined as the average time at which the speed of each digit's MCP and PM joint exceeded 10 percent of its peak speed.

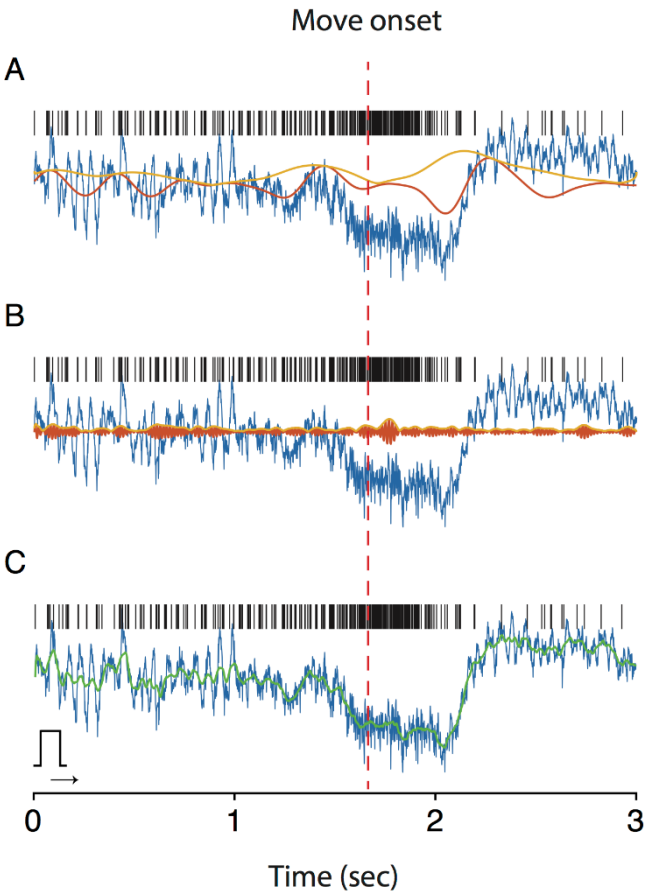

Figure 1. 4. Bandpass filtered LFP and its DC level

LFP (blue) from an example electrode during a task and the single unit activity (spike train, black) recorded in the same electrode. Band pass filtered LFP (red) and its envelop (yellow) are overlaid in (A) theta band and (B) gamma band. (C) Raw LFP's instantaneous DC level (green) is computed by convolving LFP with a box-car filter (inset).

Neurophysiology: All surgical and experimental procedures were approved by the University of Chicago Animal Care and Use Committee and confirmed to the principles outlined in the National Institutes of Health's *Guide for the care and Use of Laboratory Animals*. Each monkey was implanted with a Gray Matter 96 channel micro-drive system (GMA; Gray Matter Research, Bozeman, MT) on the left hemisphere (Figure 1.2A, B). GMA consists of a micro-drive chamber, retainer, screw guide, and actuator with 96 electrodes. Each individual electrode can be advanced/retracted using a precision screwdriver up to 32 mm deep (125 μm/turn; 1.5 mm inter-electrode distance, Figure 1.2B). GMA was placed above the central sulcus targeting the arm and hand area of both M1 and S1. The location of the central sulcus was determined based on the data from a structural MRI scan prior to surgical implantation. Anatomical research of the macaque central sulcus has shown that the position of area 3a can vary between animals, extending from the fundus into either the rostral or caudal wall of the central sulcus (Krubitzer et al., 2004). Accordingly, the GMA electrode tips probed caudal M1 and 3a by canvassing the fundus and banks of the central sulcus (Figure 1.2C).

Amplified neural signals (gain of 5000) were bandpass filtered between 0.3 Hz and 7.5 kHz and sampled at 30 kHz using the Cerebus Neural Data Acquisition system (Blackrock Microsystems, Salt Lake City, UT). Sampled signals were subsequently inspected to sort spiking activity of units using a semimanual clustering procedure (Offline Sorter; Plexon, Dallas, TX). LFP signals were separately bandpass filtered (0.3 Hz to 250 Hz) from the raw signal and resampled at 2 kHz. Only neurons with task-related response properties were used in the analyses for this study. To select the task-related neurons, we examined the neural response at two different epochs of a trial: a 200 ms window before the new object was presented by the robot arm and a 200 ms window centered around the finger movement onset. We compared the firing rate at these

two time epochs by performing a two sampled t-test and considered a neuron to be task-related if the difference in firing rates was significant at the $p<0.05$ level.

Coherence analysis: Coherence and directed coherence between neural signals sampled across different recording channels were measured using the multi-tapers method (Mitra, 2007). Coherence measures the strength of synchronized activity of two signals in the frequency domain. To measure frequency specific coherent activity between M1 and S1, we computed spike-field coherence, C_{xy}, where x is the raw spike trains of neuron and y represents the raw LFPs. Briefly, C_{xy} is calculated as the cross-spectrum of x and y (S_{xy}), normalized by the geometric mean of their autospectra, S_{xx} and S_{yy}, which can be written as following

$$C_{xy} = \frac{S_{xy}}{\sqrt{S_{xx}S_{yy}}}$$

Statistically significant coherence in the given frequency band is determined by comparing the actual coherence value to the coherence value computed with trial shuffled signals. The frequency band at which the coherence level showed the significant peak level comparing to the shuffled coherence (two sampled t-test, $p<0.05$) was deemed significant.

Information calculation: Mutual information (MI) provides a more general measure of the relationship between two time varying variables as compared to correlational methods because it can assess non-linear relationships as well. MI measures the average reduction of uncertainty about one variable due to knowledge of a second variable. If two variables are statistically independent the MI is zero (Cover and Thomas, 2012). If two variables are perfectly correlated, MI can reach a maximum corresponding to the lower entropy value of the two variables which, in our case, is determined by the measurement resolution of the variables.

In the case of somatosensory cortical neurons, the occurrence of a spike at time t is due in part to sensory signals from the sensory periphery via the thalamus and in part to the intrinsic periodicity of the neuron's firing pattern, generated by post-spike influences. In the case of some motor cortical neurons, spiking either directly or indirectly causes postsynaptic effects on motor neurons in the spinal cord which directly affect muscles and motor behavior. To examine recorded cortical neurons' task modulation and its first order temporal latency, we measured MI between time varying joint kinematics and a given neuron's response at different temporal latencies. More specifically, we measured the MI between each joint kinematics at time t (N(t)) and a given neural response at time t+Δt (θ(t+Δt)), varying Δt to determine the most informative time delay between the neural response and joint the kinematics, which is written as

$$I(N_t;\theta_{t'}) = \sum_{N_t,\theta_{t'}} P_N(N_t)P(\theta_{t'}|N_t)\log_2\left(\frac{P(\theta_{t'}|N_t)}{P_\theta(\theta_{t'})}\right)$$

where t' = t+Δt and Δt ∈ [-200, 200] ms with 20 ms time increment.

Model: To characterize the functional connectivity between pairs of cortical sites, we used a statistical regression modeling approach, Generalized Linear Model (GLM). The GLM attempts to predict the number of spikes emitted from neuron A in one cortical area in the present time bin (size of 1ms) based on three types of covariates (predictors): 1) the LFP from another recording channels, $g_{LFP}(t)$; 2) the kinematics of the hand at multiple time leads/lags, $g_{Kin}(t)$; and 3) the base line firing rate of the neuron, β. The instantaneous firing rate λ(t) of target neuron A can be estimated as:

$$\lambda_{Full}(t) = F(g_{LFP} + g_{Kin} + \beta) \quad (1)$$

where F(·) is a nonlinear function. Previous studies from our group, that focused on upper limb movement encoding of M1 successfully implemented the GLM with an exponential nonlinear

function (Saleh et al., 2010, 2012; Takahashi et al., 2017). To emphasize the neuron's encoding in terms of extrinsic covariates (i.e. kinematics and LFPs from other recording sites), we didn't consider intrinsic covariates in the model such as absolute and relative refractoriness of the neuron, and intrinsic oscillations, realized by spike-history terms of GLM. Unless otherwise noted, the above model (equation 1) will be denoted as the FULL model as it contains all covariates of the model we considered in this study. Each component of the model includes a parameter matrix to be fitted to the data. With the exponential nonlinearity in the model, we attempted to fit the model by maximizing log-likelihood of the data given the set of parameter structures. The log-likelihood of the observed spike times given the parameters is as following:

$$\mathcal{L} = \sum_{t_s} \log \lambda_{t_s} - \int \lambda \, dt \tag{2}$$

where t_s indicates the time bins where spikes occurred.

Performance measure: We used the fraction of variance accounted for (FVaF) of the observed firing rate of the target unit by the model's generated firing rate. FVaF is defined as following.

$$FVaF = 1 - \frac{\sum_{i=1}^{N}(y_i - \hat{y}_i)^2}{\sum_{i=1}^{N}(y_i - \bar{y})^2}$$

, where y is a true firing rate, $\hat{y}$ is the model's prediction, and $\bar{y}$ is a mean firing rate. Each instantaneous firing rate is calculated by convolving the spike train with a Gaussian kernel (SD = 16 ms). 10 folds of cross-validation were used to avoid overfitting in our regression model (i.e., 10% of total data was used to test the model built on 90%of remaining data).

Local field potentials variables: To represent the cortical interaction from one site to another, the LFP signal from one electrode was used to predict the neuron's spiking activity recorded on

another electrode. The LFP implementation in the GLM is similar to that of used in Cui et al. (Cui et al., 2016): all LFP signals were bandpass filtered at gamma (50~85 Hz) and theta (4~7 Hz) frequency bands and their instantaneous energy w(t) (that is, the amplitude of the filtered LFP envelope) and phase φ(t) were used as covariates in the model. We applied the Hilbert transform to compute w(t) and φ(t) for each band pass filtered signal (Le Van Quyen et al., 2001). The LFP signals was then expressed as a linear combination of cosine and sine functions, modulated by w(t) and φ(t) as following:

$$\overline{g_{LFP}(t)} = \sum_{f_i} a_{f_i} w_{f_i} \cos(\varphi_{f_i}(t+\tau)) + b_{f_i} w_{f_i} \sin(\varphi_{f_i}(t+\tau))$$

where f_i includes 2 frequency bands listed above and τ is time lag between the target electrode where we sampled the spiking activity of the neuron and the electrode where we sampled the LFP signal. Other frequency band ranges, such as alpha (8~13 Hz) and beta (15~30 Hz), were excluded from the analysis for the following reasons: (1) across all epochs of the trial, no substantial spike-field coherence were observed, (2) the beta frequency component of the LFP is suppressed and little to no substantial beta power is observed during hand movement (O'Leary and Hatsopoulos, 2006), and (3) regression models that involve model parameter optimization tend to perform better with fewer number of covariates. We observed that the DC level of the LFP recorded from both M1 and S1 varied across different epoch of the task (Figure 1.4C). The firing rate of a single unit recorded from the same electrode was closely related with the LFP's DC level and conventional filtering of the LFP didn't reflect this apparent relationship with spiking activity of neuron (Figure 1.4A,B). To account for this relationship between the LFP DC level and the single unit's firing rate, the DC level of raw LFP signal (L_{DC}) was also used as additional covariate in the model. $L_{DC}(t)$ is computed as average raw LFP value of each sliding time window with width of 100 ms. Therefore, the LFP components of the GLM model were expressed as following:

$$g_{LFP} = \overline{g_{LFP}} + c \cdot L_{DC}(t + \tau)$$

Optimal lag between recording sites: To compute the optimal time lag (τ) between recording sites, we used a variant of the full model. In this model scheme, only the LFP term g_{LFP} and the baseline firing rate term are included as covariates in the GLM as following.

$$g_{LFP}(t) = F(g_{LFP} + \beta) \quad (3)$$

For a given target neural spiking response and the LFP activity recorded from another electrode, we measured model performance of g_{LFP} varying τ (0~200 ms, 5 ms increment time step) in the LFP term g_{LFP}. After fitting the model (equation 3) to the data, the time delay (τ) that resulted the highest model performance on test data was selected as the optimal time delay between two sites.

Joint kinematic variables: We used both position and velocity of 23 joints of the hand at multiple time lags as input features to our encoding model. 12 time lags were used from -300 ms to 300 ms with respect to the spike time (50 ms time step). The resulting external covariates based on the joint kinematics in the model was formulated as:

$$g_{Kin} = \sum_{m} \sum_{r} d_{m,r} \cdot K_r$$

where K_r is time varying rth joint kinematics and $d_{m,r}$ is center-shifted Gaussian basis vectors whose amplitude was determined by the GLM for each joint r and different time delays $m \in$[-300,300] .

Model fitting and regularization: We used a regularized regression (LASSO GLM) approach to identify the functional response field (i.e. receptive and/or projection field) of the neuron in M1 and S1. During hand grasping, the time varying joint angular positions/velocities of each joint

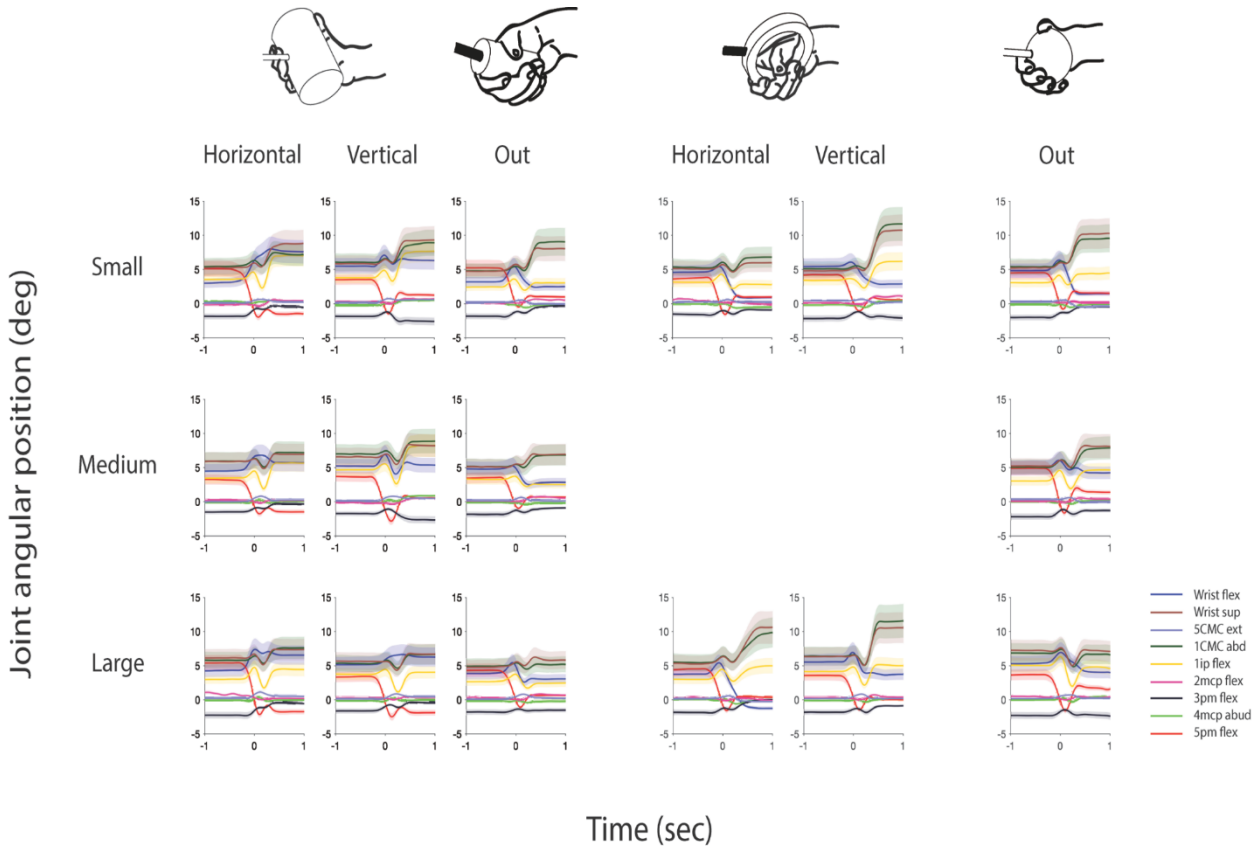

Figure 1. 5. Example joint angular positions across objects

Joint angular position trajectories for example objects around movement onset.

were highly correlated, suggesting that a few joint kinematics may be adequate to account for most of the variance explained. To overcome overfitting, it is highly advantageous to choose only relevant kinematics (features) to the given neuronal response and use only a subset of kinematics to build the predictive model as we have limited amount of data in a model with very many parameters (joint terms + baseline firing rate term = 553 parameters in the encoding model for each neuron). LASSO regularization accomplishes this and together with cross-validation, we were able to overcome overfitting. To infer the response field of given neuron, we used the so-called reduced model that only contained joint kinematic term g_{Kin} and the baseline firing rate term

$$\lambda_{Reduced}(t) = F(g_{Kin} + \beta) \quad (4)$$

. LASSO regularization was applied to the reduced model by adding the prior belief of the feature distributions or "penalty term" to the log-likelihood calculation of (2). In the context of LASSO regularization, we used the Laplace prior distribution, M, as follow:

$$P = L - M = L - \alpha \sum_i |d_i| \quad (5)$$

where α is a hyper-parameter that determines the degree of the penalization. The model fitting can be proceeded by maximizing P with a given set of parameters and the set of input and output data. α is selected by cross-validation on the test dataset that resulted in the best model prediction. Generally, optimizing equation (5) using gradient-based method is not advised as computing the gradient and Hessian of M at the origin is not possible. In this study, we used continuous approximation of M to compute the gradient and Hessian at the origin (Schmidt et al., 2007), enabling the use of gradient-based optimization method.

Results

Seven recording sessions (i.e. datasets) were collected and analyzed from 2 monkeys (4 sessions from monkey J and 3 sessions from monkey B). For each session, at least 10 trials of each combination of object kind/size/orientation were presented (a total of at least 350 trials/session). Neural and hand joint kinematic data were collected while the monkey was engaged in the grasping task (see Materials and Methods for details). In a given day and before collecting data, we advanced or retracted all electrodes of the GMA in an attempt to search for clearly isolated single units. On the site of recording, crude measurements were used to identify grasp related

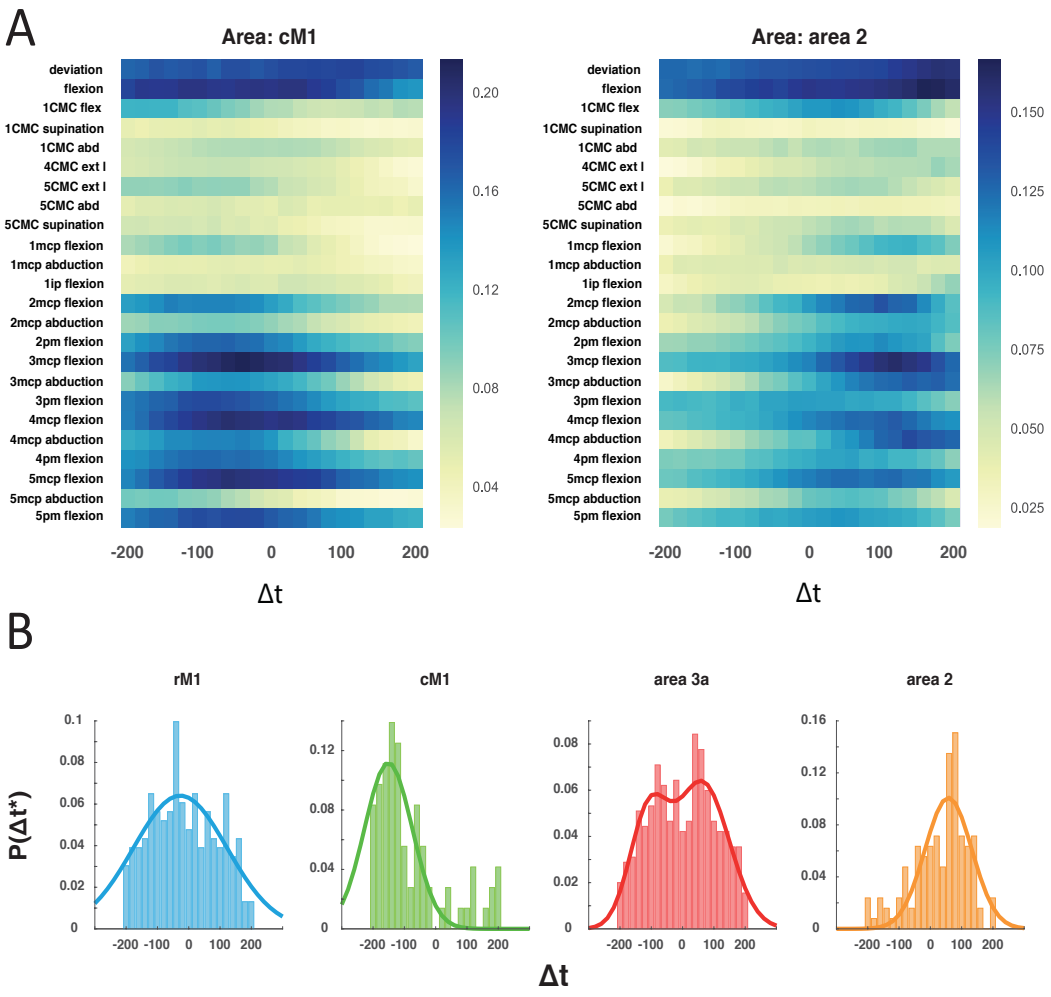

Figure 1. 6. Neural latency analysis using mutual information calculation

(A) Mutual information between angular velocity of various joint and spike train of example cM1 neuron (left) and area 2 neuron (right) with respect to the time shift (Δt) in the spike train. (B) Distribution of Δt at which we observed peak mutual information between neurons in rM1 (blue, n= 49), cM1 (green, n=30), area 3a (red, n=33), and area 2 (orange, n=24) and all joint kinematics.

proprioceptive, cutaneous (for S1), and motor (for M1) units. For S1 units, the animal's hand joints were passively stimulated to monitor neural modulations. For M1 units, the experimenter handed objects to the animal to be grasped and neural modulations were monitored. We analyzed 102 paired sites from monkey J and 78 paired sites from monkey B.

It is evident that the animal used different grasping strategies across different object conditions (Figure 1.5). Figure 1.5 shows examples of mean traces (aligned on finger movement onset) of the wrist flexion, supination, 5 CMC extension, 1 CMC abduction, 1 ip flexion, 2 mcp

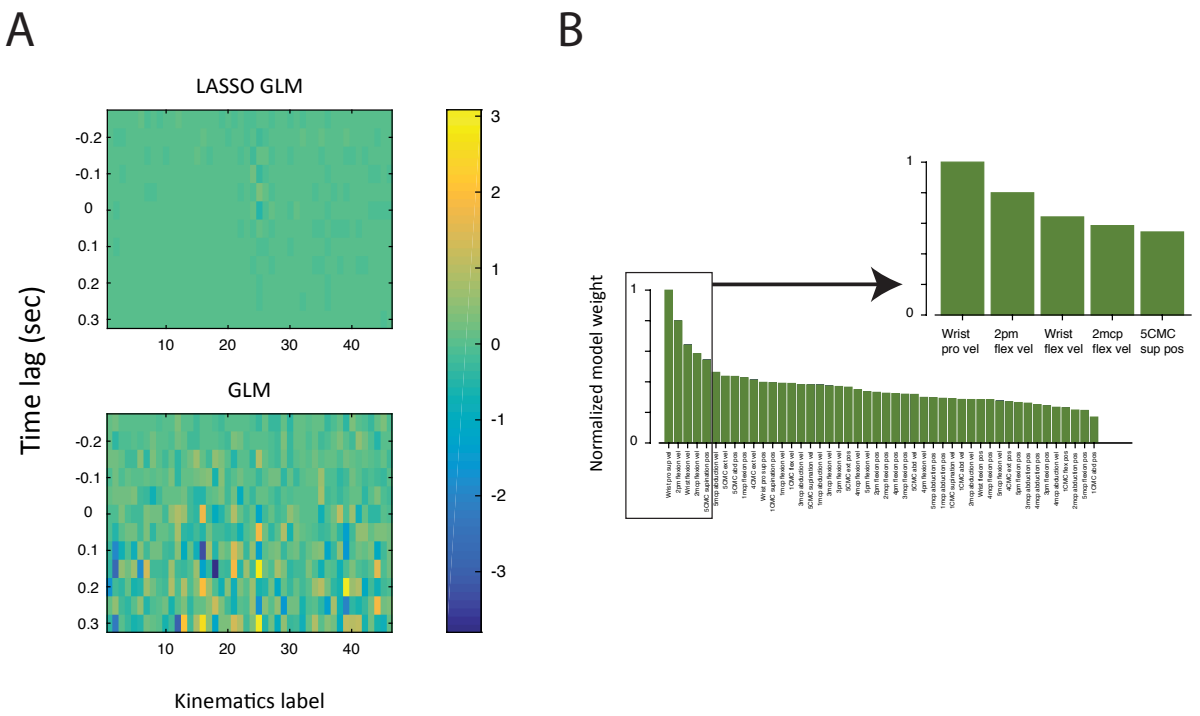

Figure 1. 7. Mapping functional receptive field of single neurons
(A) Example of inferred model weight for joint kinematics predictors computed using LASSO GLM (up) and regular GLM (down) against the same neuron and joint kinematics data. (B) Visualizing LASSO model weights for hand joint kinematics. Model weight parameters computed in (A) are summed across time lag axis and normalized and sorted for measuring relative contribution for prediction. Given neuron's feature vector is constructed based on LASSO model weight.

flexion, 3 pm flexion, 4 mcp abduction, and 5 pm flexion for different grasping conditions. Among the selected joints, the wrist joints showed the most pronounced differences across the object types on average. By visually inspecting the animals performing the grasping task, monkey J showed more diverse set of wrist supination and pronation movement strategies across different objects, which further directly affected different strategies for various hand grip postures. Monkey B displayed more stereotypic grasping strategies across all task conditions and his maximum grasp apertures were significantly bigger than monkey J.

	M1 to S1	S1 to M1
Monkey J	43.25 ± 2.44 ms	35.64 ± 2.77 ms
Monkey B	52.8 ± 9.74 ms	40.82 ± 6.84 ms

Table 1. 1 Corticocortical connection delays between M1 and S1 computed by GLM.

Neural-Behavioral Latency: To investigate each neuron's response latency to hand grasping behavior, we measured the mutual information (MI) between each joint kinematics at time t and given neural response at time t+Δt, varying Δt from -200 ms to 200 ms in 20 ms time increments. In the joint kinematics data, we focused on flexion, extension, abduction, and adduction movement of finger joints and discarded most distal finger joints in the information calculations because the animal does not have voluntary control over the distal finger joints. The example MI curves in terms of time delay for M1 and S1 neurons are shown in Figure 1.6A. Each neuron's response selectivity in time was evident with a single peak in the MI curve across a few neighboring digits. We pooled all information curves computed for each joint and constructed a histogram of latencies of peak information across all neurons within an area (Figure 1.6B). Only curves with clear peaks were investigated for this analysis (Gaussian fit, $R^2 > 0.9$). The unimodal distributions of peak MI time latencies for both rM1 and cM1 were unimodal with a mean and mode at negative time indicating that on average neural responses preceded hand kinematics. On the other hand, the distribution of peak MI latencies for area 2 was unimodal with a mean and mode at positive time indicating that on average these neurons' responses followed the kinematics. Finally, the distribution of peak MI latencies in area 3a was better described as bimodal with one positive and one negative time mode suggesting a mixture of sensory and motor-like responses.

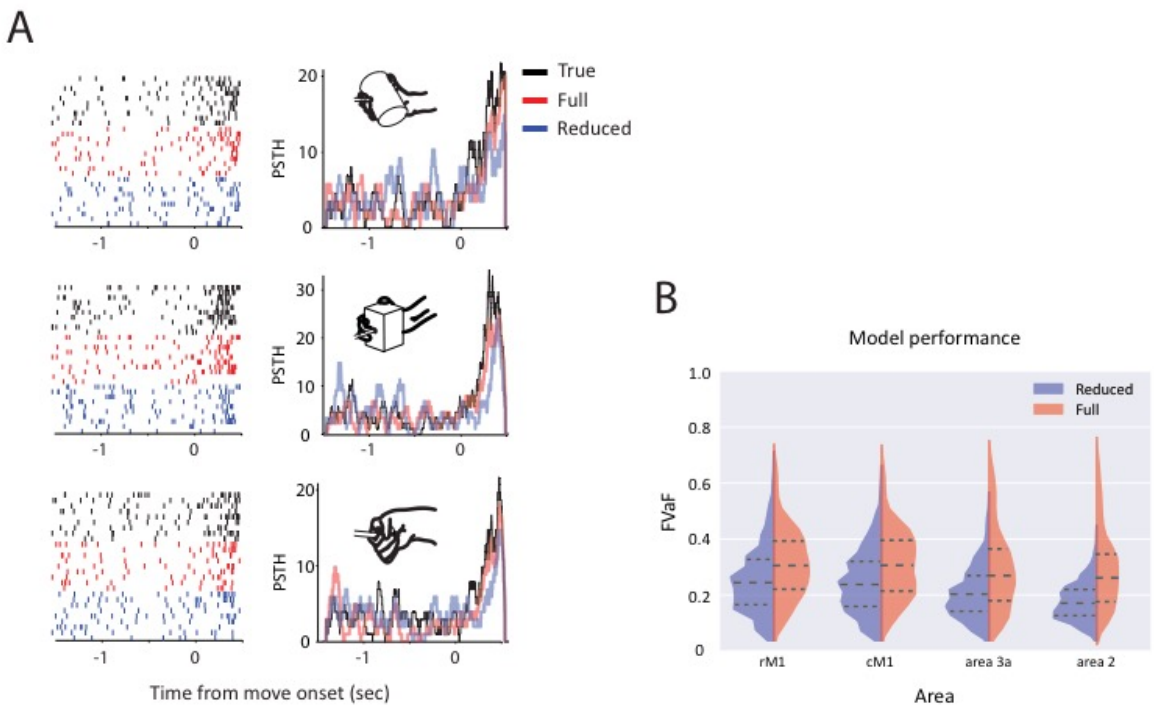

Figure 1. 8. Model performance comparison
(A) Raster plot and PSTH for true spiking (black), full model prediction (red), and reduced model prediction (blue) for 3 different object presented (inset). Model performance was measured using R-squared between true firing rate and model generated firing rate. Presented full model's R-squared is 0.7664 (cylinder object), 0.7179 (block object), and 0.6375 (sphere object) and reduced model's R-squared is 0.431 (cylinder object), 0.4539 (block object), and 0.3549 (sphere object). (B) Model performance comparison between full model (red) and reduced model (blue) across all neurons we tested, rM1 (n= 49), cM1 (n=30), area 3a (n=33), and area 2 (n=24).

Encoding Model: We employed an encoding model that predicts a single neuron's firing rate (output) with a given set of covariates (input) using a generalized linear model (GLM) (Saleh et al., 2010, 2012; Takahashi et al., 2017). We developed 3 different classes of GLMs to (1) map the kinematic response field (RF) of single neurons by using 23 joint kinematics with multiple time lags as a set of covariates (2) infer the optimal time lag between a single neuron recorded on one electrode and the band-pass filtered LFP recorded on another electrode, and (3) describe the functional connectivity between two sites by predicting a single neuron's response using the band-pass filtered LFP recorded on another site together with the joint kinematics as covariates. In order

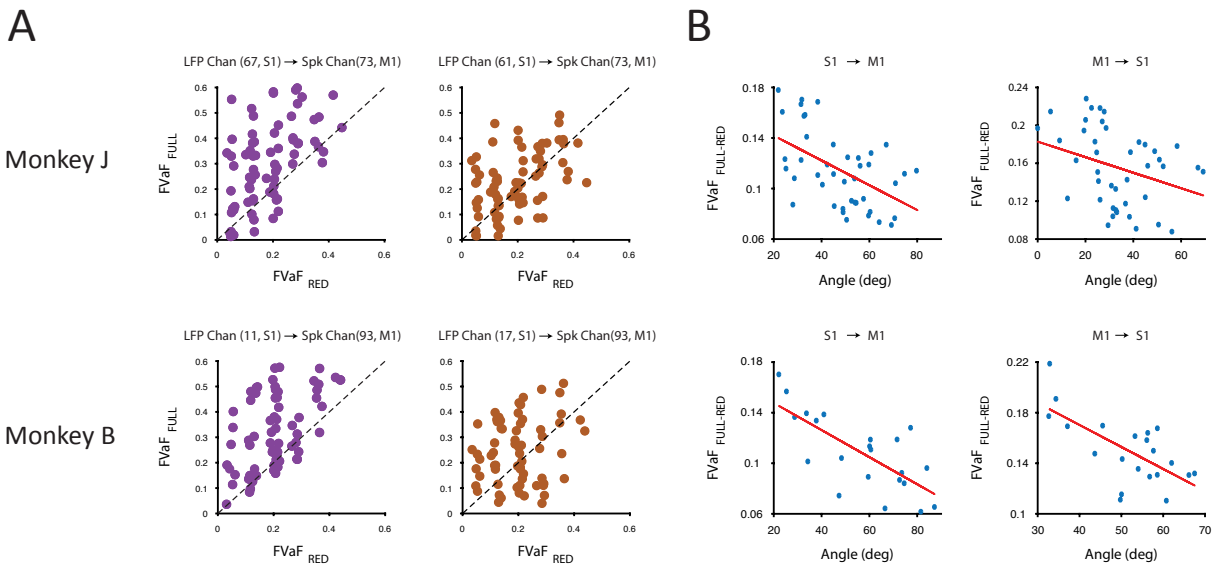

Figure 1. 9. Measuring model performance improvement via LFP and its relationship with neurons' functional property

(A) Model performance comparison (Full vs. Reduced) of example pairs. Left column represent significant model improvement and right column shows non-significant model improvement ($p<0.02$, Wilcoxon rank sum test). (B) Relationship between pairs of cortical sites that showed significant model improvement and their receptive field organization. Systematic relationship between the performance improvement of the FULL versus REDUCED models and the angle between pairs of neurons' joint kinematic feature vector. Linear fit of data is plotted in red. The r-values of regression in monkey J (up) are 0.255 (S1 → M1) and 0.105 (M1 → S1) and in monkey B (below) are 0.521 (S1 → M1) and 0.45 (M1 → S1).

to measure the model performance, we computed the fraction of variance accounted for (FVaF) of the actual firing rate of the neuron by the model (See Methods).

Mapping Response Fields: Each neuron's response field (RF) was estimated using regularized GLM (LASSO) and investigating the parameters associated with the covariates. Both angular position and velocity of each joint with multiple time lags ($\Delta t \in$ [-300,300] in 50 ms time steps) were used as input covariates in the model. To validate LASSO model fitting, we used a simple generalized linear model without regularization to fit the same datasets and compared the model structure (Figure 1.7A). Fitted parameter weights for both models are plotted for an example neuron in Figure 1.7A. Although their predictive performances were not significantly different (p

< 0.05, Wilcoxon rank sum test, data not shown), the inferred model parameter values showed clear differences (Figure 1.7A). We then summed the parameter values across the time lag dimension to investigate each feature's relative contribution to the model fitting. Figure 1.7B shows normalized parameter values for an example neuron model in descending order. For most cases, several joint features had parameter values that were significantly higher (thus, contribute to model fitting significantly) than others (Figure 1.7B inset).

Inferring Cortical Communications: To investigate cortico-cortical interactions between recording sites during the grasp, we employed LFP signals from one recording site to predict the spiking of a neuron recorded from another site using a GLM. It is known that only some frequency components of the LFP signal are better correlated with local cortical neural activity (Cover and Joy, 2012). For this study, we considered two frequency bands of the LFP to build the GLM: theta (4~7 Hz, Figure 1.3B, Figure 1.4A) and gamma (50~85 Hz, Figure 1.3B, Figure 1.4B). These frequency ranges were chosen based on the presence of substantial spike-field coherence in these frequency bands (Arce-McShane et al., 2016) at around the hand movement onset time (Figure 1.3C, shuffled test, two sample t-test, $p < 0.05$) for both M1 and S1. Other frequency band ranges, such as alpha (8~13 Hz) and beta (15~30 Hz), were excluded from the analysis for the following reasons: (1) across all epochs of the trial, no substantial spike-field coherence were observed, (2) the beta frequency component of the LFP is suppressed and little to no substantial beta power is observed during hand movement (O'Leary and Hatsopoulos, 2006), and (3) regression models that involve model parameter optimization tend to perform better with fewer number of covariates. We also observed that the raw LFP (unfiltered) signal's amplitude reflected the state of single

neural activity (i.e. firing rate) recorded from the same electrode (Figure 1.4C) and was included as a covariate together with the two band-pass filtered LFP signals.

We first sought to find the optimal time lag of cortical communication between LFP-spiking pairs recorded from different cortical sites. In this analysis, we used a GLM that predicts a target neuron's spiking activity with only the LFP input from another recording site (Equation 3). Because we considered different time delays between the sites, the time lag (τ) term acted as a hyper-parameter in the model. The optimal time lag was determined as the one that resulted the highest model performance (i.e. largest FVaF on test data). The estimated time delays between M1 and S1 were consistent across monkeys showing a clear tendency for longer time delays from M1 LFPs to S1 spiking as compared to S1 LFPs to M1 spiking. The inferred time delay data is given in Table 1.

We proceeded to measure the performance of the FULL encoding model (Equation 1) and REDUCED encoding model (Equation 4). Across all animals and brain areas, we found that the full model moderately improved model predictability compared to the reduced model. The raster plots and corresponding PSTH of model simulations for an example neuron-LFP pair are shown for each of 3 objects presented (Figure 1.8A). The REDUCED model alone, accurately predicted the timing of neural modulation of grasping. The FULL model further improved the firing rate predictability not only with more precise timing of neural modulation but also with more accurate numbers of spikes around movement onset time. Across all brain areas, we found that the median FVaF values for the FULL and REDUCED models were 0.3394 and 0.2063, respectively. In both animals, we observed that both the REDUCED and FULL models for M1 neurons performed better than those for S1 neurons (REDUCED model: median of 0.2279 (M1) vs 0.1921 (S1) for monkey J and 0.2251 (M1) vs 0.1952 (S1) for monkey B; FULL model: median of 0.3448 (M1) vs 0.3009

(S1) for monkey J and 0.3524 (M1) vs 0.2828 (S1) for monkey B). In terms of the model performance in sub-regions of M1 and S1, rM1 neuron models performed better than cM1 neuron models and area 3a models outperformed area 2 neuron models (Figure 1.8B).

To measure functional connectivity between cortical areas, we tested whether the LFP recorded in one area together with the kinematics (FULL model) provided more information about the spiking activity recorded in another area than the information provided by the kinematics alone (REDUCED model). If the FULL model showed significant improvement in model performance, we assigned a functional connection between the LFP site and the spiking neuron site (Figure 1.9A, left column, Wilcoxon signed rank test, $p < 0.02$). On the other hand, if the FULL model didn't show a significant improvement, we considered the two sites to not be functionally connected (Figure 1.9A, right column).

Finally, we tested if there was any systematic relationship between the performance improvement of the FULL versus REDUCED models ($FVaF_{FULL\text{-}RED}$) and the RFs of the corresponding sites. To this end, we used the feature selectivity structure that we mapped using LASSO GLM in the Mapping Response Field section and constructed a 46-dimensional joint kinematic feature vector for each neuron reflecting each neuron's preferred set of kinematic features in multi-dimensional kinematic space (see Methods) and compared $FVaF_{FULL\text{-}RED}$ with the angle between the two feature vectors (referred to as the dissimilarity in RFs) of the corresponding neurons in the two sites. In both monkeys, we found a strong negative correlation between dissimilarity of the neurons' RFs and their functional connectivity (Fig 1.9B).

To investigate the possibility that common input to both sites could explain the FULL model's improvement among pairs with similar RFs, we performed an analysis that compared the cortical time lag between paired sites with similar RFs and the difference in neuron-behavioral

latencies. We used each neuron's latency to behavior that we computed in the previous section using information theoretic analysis. We found that there was no systematic relationship between the cortico-cortical time lag of a given pair of sites and the difference in neural-behavioral latencies of the two neurons (p=9.77e-5, Wilcoxon signed rank test). Therefore, at least in our datasets, we can rule out the possibility that common input contributes significantly to the FULL model improvement among pairs with similar RFs.

Discussion

We found that neurons in the hand area of M1 and S1 encode kinematics both position and velocity of the hand joints. Neurons' response fields in both M1 and S1 exhibited a broad range of sizes and locations on the hand. By statistically analyzing functional interactions between the spikes and the LFPs recorded across the areas, we found that M1 and S1 sites that shared similar RFs exhibited stronger and more numerous functional connections than pairs with dissimilar RFs. Our results suggest that cortical connectivity structure may facilitate the synergistic coordination of hand motor control.

LFP in the sensorimotor cortical area: The LFP is the summed activity of local network neurons and it is likely influenced by multiple sources of synaptic inputs (Khawaja et al., 2009; Einevoll et al., 2013). Different source of fluctuations can be identified as distinct frequencies in the signal and band-pass filtered LFP can provide selective information about the network. Our spike-field coherence analysis revealed that neural activity in M1 and S1 is well represented in the theta band (4~7 Hz) and gamma band (60~85 Hz) of LFP. Our group recently also reported prominent reciprocal interactions between orofacial motor and somatosensory cortices in theta and gamma

frequency bands (Arce-McShane et al., 2016). A high correlation between single neuron activity and gamma band oscillation has been previously reported in various different brain areas (Nir et al., 2007; Bruns et al., 2010; Buzsáki and Wang, 2012; Jia et al., 2013). One of the known functions of gamma oscillation is characterized as coordinated interactions of excitation and inhibition (Buzsáki and Wang, 2012), which may have played a role in the interareal interactions. The main function of theta band oscillation is not clear yet, though previous studies in the arm M1 and S1 interaction suggest that theta synchrony is organized according to movement phases (Feige et al., 2000; Ohara et al., 2001). Evidence of an association between theta band oscillation and working-memory and reward expectation has been previously reported (Lee et al., 2005; Li et al., 2017).

Inference of neural latency using mutual information: We found that various neural-behavioral latencies in sensorimotor cortical neurons (Figure 1.6B). It is expected that M1 neurons should generally lead joint kinematics. However, the neural-behavioral latency distribution for area 3a neurons was best described as a bimodal distribution with peaks at both negative and positive latencies. Rathelot and Strick's finding that some area 3a neurons as well as many cM1 neurons send direct and monosynaptic projections to motoneurons in the spinal cord (Rathelot and Strick., 2008) suggests that area 3a neurons may contain a subpopulation of neurons that show motor-like response (time-lead) as well as another subpopulation of neurons that show sensory-like response (time-lag).

Mapping somatotopy using regularized GLM: Although mutual information is a common method to measure non-biased dependency structure between two variables (time series), it is non-parametric and shows weakness in measuring the relative contribution of multiple predictors to the

dependent variable, especially when the independent variables are highly correlated. Since our joint kinematics displayed high correlation, we instead, used a parametric linear regression method, LASSO GLM, to measure the feature importance of the model (Figure 1.7). LASSO is particularly used when model fitting involves many predictors (Pillow et al., 2008; Calabrese, Ana, et al., 2011; Cui et al., 2016).

Our LASSO GLM analysis revealed that neurons in M1 and S1 carry significant information about not a single joint, but multiple joint kinematic features (on average, 4 joints) selected by thresholding the model's parameter values. We found that when LASSO selected features are used to predict the spiking activity of a neuron, it outperformed other possible joint kinematic sets we tested (data not shown). Thus, LASSO selected features for a given neuron was used for further analysis of functional communication between areas.

Somatotopically organized functional interactions between areas: Cortico-cortical connections in terms of cortical neurons' functional organization has been investigated in the visual system (Cleland et al., 1971; Ts'o et al., 1986; Hata et al., 1991; Salin et al., 1992) and the sensorimotor system in cats (Asanuma et al., 1968; Thompson et al., 1970, Asanuma et al., 1982; Herman et al., 1985). These studies provide partial evidence of retinotropically (visual cortex) and somatotopically (sensorimotor cortex) organized connectivity structure. Our results also show a consistency with previous studies mentioned above: we found that sites between M1 and S1 that had similar RFs (i.e. similar somatotopic representations) were more likely to be functionally connected.

The exact function of these functional connections between M1 and S1 is unknown. However, there are number of studies that investigated the characteristics of connections between

M1 and S1 in rodent (Farkas et al., 1999; Rocco-Donovan et al., 2011) and cats (Sakamoto et al., 1987; Iriki et al., 1991). In particular, their studies suggest that connections from S1 to M1 are modulatory signals closely related with motor learning. However, it is unlikely that the connections we found serve this purpose. Both our monkeys had been exposed to the grasping task for more than 2 years ago and had attained proficiency in the task before we had begun these experiments which indicates that motor learning was no longer taking place. A more plausible function of these connections is that they may facilitate the synergistic coordination of movement with sensation.

Chapter 3: Interactions between primary motor and somatosensory cortices in the macaque during grasp using intracortical microstimulation

Abstract

Recent studies in neuro imaging using diffusion imaging tractography have reported direct association fibers between primary motor (M1) and somatosensory (S1) cortical areas in the living human brain. However, their functional significance is largely overlooked in the major sensorimotor transformation model, especially in the model of visually guided hand grasping. Here, we used multielectrode arrays implanted in M1 and S1 to investigate the effect of intracortical microstimulation (ICMS) applied at one electrode on the responses of neurons recorded on other electrodes while monkeys engaged in grasping task and in the resting state. We found excitatory connections between sites within a cortical area whose amplitude and latency depended on inter-electrode distance as well as non-random and reciprocal excitatory and inhibitory connections between M1 and S1. We observed a strong correlation between the sign of the connections and the response fields of neurons in M1 and S1. We also found evidence that communications between M1 and S1 were highly plastic and depended on the animal's behavioral state. Our results suggest that functional connections between M1 and S1 facilitate the synergistic coordination of movement with sensation.

Introduction

Prehensility, the ability to grasp, affords us a great advantage in surviving and manipulating objects. As such, the neural mechanisms of grasping behavior has been extensively studied. Many brain areas are involved in generating visually guided grasping behavior. Sensory information serves to locate and measure the affordability of grasping (i.e. object to grasp and effectors), which involves in visual cortex, somatosensory cortex, and intraparietal area, especially anterior intraparietal area (AIP) for hand behavior. Then, internal model of kinematic and kinetic are created and precisely planned to execute the movement. Area F5 in the ventral premotor cortex (PMv) and the primary motor cortex (M1) are largely involved in this stage. In the current model of grasping circuit, these areas are sequentially activated (in parallel, however, for many cases) to generate the motor behavior. It is surprising, however, that connection between M1 and the primary somatosensory cortex (S1) has been largely overlooked in the model of generation of grasping behavior.

The existence and function of connections between M1 and S1 have been examined using anatomical tracing method (Jones et al., 1978) and more recently, optogenetic imaging technique (Rocco-Donovan et al., 2011; Petrof et al., 2015; Kinnischtzke et al., 2016), and diffusion imaging tractography (Shinoura et al., 2005; Catani et al., 2012). Catani and colleagues showed that the associative fibers between M1 and S1 in human boast the greatest volume and size among other fibers they investigated but the functional role of such connections is yet to be discovered. The spatial structure of connections between sensorimotor cortex was studied in cats (Asanuma et al., 1968; Thompson et al., 1970, Asanuma et al., 1982) first in the anesthetized cat using a combination of intracortical microstimulation (ICMS) and electromyographic techniques which confirmed that many recorded neurons in pericruciate cortex (72%) send impulses to a common

motoneuron pool and receive cutaneous information from a localized skin region. Using ICMS technique, Thompson et al. (1970) found that the population of neurons in S1 which receive input from a specific peripheral locus send projections to a region of M1 which receives sensory input from the same or a contiguous locus.

Although the above studies have shown evidence of anatomical and functional interactions between M1 and S1, how this communication structure is organized and functions in the context of an ethological behavior is yet to be elucidated. Here, we tested the hypothesis that causal interactions between M1 and S1 in macaque are somatotopically organized during a grasping task such that sites in M1 and S1 that interact with excitatory connections are more likely to share similar receptive/projection fields (RFs/PFs). Low intensity biphasic current pulses were delivered through a electrode while we record the responses of neurons in M1 and S1 in the multi-electrode array setup, while monkeys engaged in a grasping task. We found sparse but significant and reciprocal connections between M1 and S1 that dynamically changed its mode with respect to the subject's behavioral states. Significant corticocortical connections are organized in terms of neurons' functional property such as receptive or projection field of a neuron. Together, we provide the evidence of synergistic communication structure between M1 and S1 during the motor task.

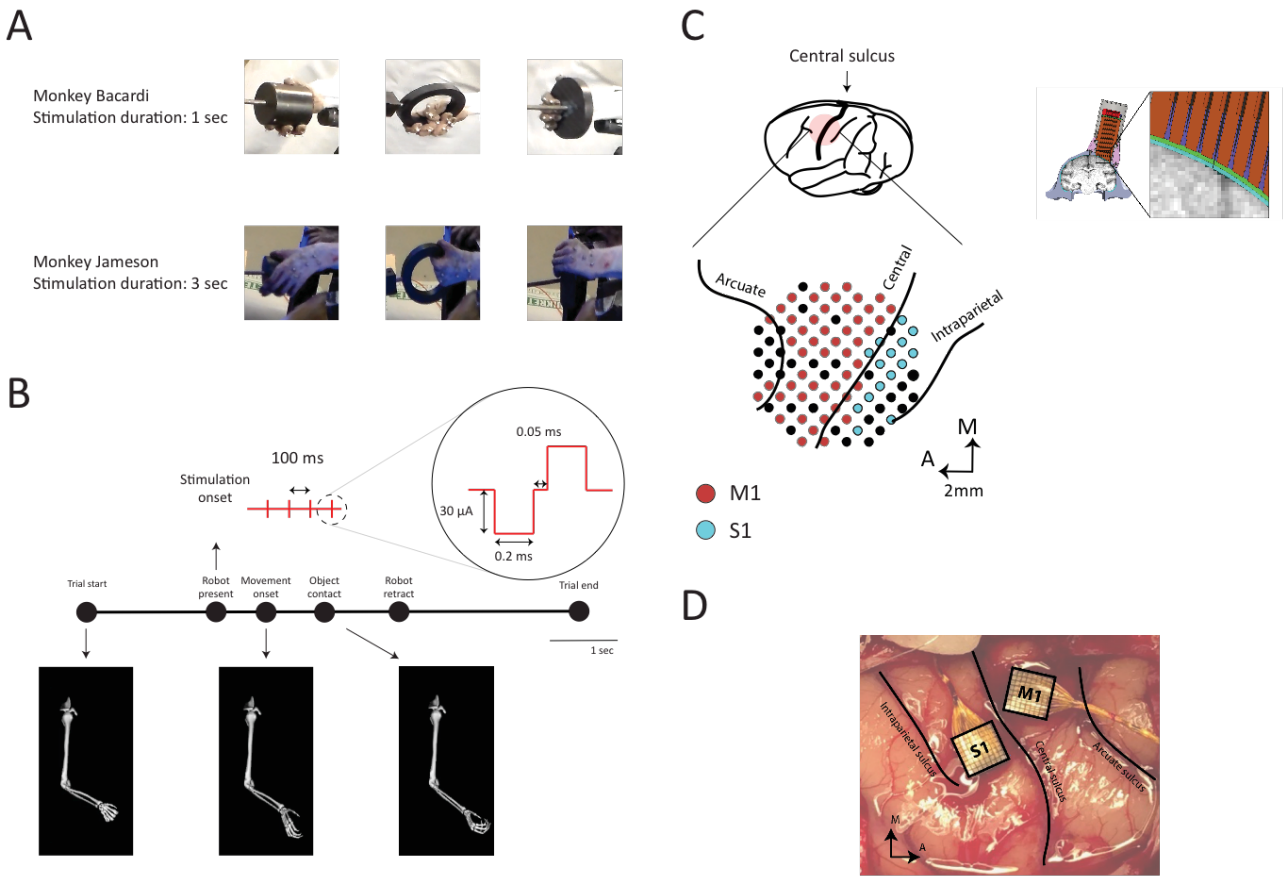

Figure 2. 1. Behavioral task and neural recording setup
(A) 3 objects presented for each monkey. L cylinder H, L ring V, and L disk for monkey B and L cylinder O, L ring V, and S block V for monkey J. (B) Task timeline. The trial started as the robot started to move the object towards the subject's hand. As the robot moved closer to the hand, the subject pre-shaped his hand to grasp the object. The subject was instructed to hold the object until the robot retracted it at which point the hand released the object. ICMS onset is locked to the robot present moment. The single pulse stimulation pattern consisted of 10 pulses for monkey B and 30 pulses for monkey J per trial (0.2 ms biphasic, cathode first, 30 µA) delivered at 10 Hz. (C) Location of placement of Gray-matter microdrive system in monkey B (left) and a view from anterior side (right). Individual electrode can be advanced and retracted up to 32 mm depth. (D) In monkey J, Utah arrays were implanted into M1 and S1.

Materials and Method

Behavioral task: Two subjects (rhesus macaques, monkey J and B) were trained to grasp objects with their hand (right hand for monkey B and left hand for monkey J). The behavioral task was described in the previous chapter. Briefly, each subject was trained to sit in a custom designed monkey chair with armrests on which the subjects were trained to place their arms. Light diode

sensors were placed under the armrests and detected if the subject maintained its arms on the armrests. Once the monkey maintained a preparatory posture, which was triggered by the complete coverage of the light sensor diodes with its arm, the animal was presented with an object by a robotic arm (Mitsubishi RV-1A-SI1, Tokyo, Japan) and grasped the object. A pseudorandom delay interval (0.5~1.5 sec) was applied after the initial grasp and the retraction of the object by the robot back to its initial position. Subjects were required to maintain a firm grasp and were rewarded for successful holding and detaching the object from the robotic arm. If, at any time point during the trial, the subject did not maintain contact with the armrest or detached the object prior to the retraction of the robotic arm (that is, detaching the object by pulling his arm), the trial was aborted. We pre-selected 3 objects from 35 different objects used for the previous study (Chapter 1) for each monkey. We used a K-nearest neighbor clustering algorithm on their joint kinematics data collected in the previous study to select 3 objects that showed the most distinctive grasping behavior. The three pre-selected objects were: a large cylinder, a horizontally oriented large ring, and a large disk for monkey B, and a large cylinder, a vertically oriented large ring, and a vertically oriented small block for monkey J (Figure 2.1A). On average, each subject completed 70 repetitions of each object presentation per session.

Motion tracking: In one subject (monkey J), motion tracking was performed using a 14 camera Vicon motion tracking system. The system tracked the three-dimensional positions of reflective markers (3 mm diameter) attached to the subject's first and second digits of the hand (Figure 2.1A, bottom). From these 3D coordinates, joint kinematics were reconstructed as function of time using a model of the primate forelimb in OpenSim (Delp et al., 2007) (Figure 2.1B). A total of 6 markers were used to compute 3D coordinates of the first and second digit of the hand: first digit

metacarpal-phalangeal (1 MCP), first digit inter-phalangeal (1 IP), 2 MCP, and 2 proximal mid (PM) joints. The kinematic data were sampled at 100 Hz and bi-directionally filtered with a fourth-order Butterworth low-pass filter with 6 Hz cut off frequency. All data filtering and computations were done in MATLAB (The MathWorks, Inc., Natick, MA). The finger movement onset time was determined as the average time at which the speed of each digit's MCP and PM joint exceeded 10% of its peak speed.

Neurophysiology: All surgical and experimental procedures were approved by the University of Chicago Animal Care and Use Committee and confirmed to the principles outlined in the National Institutes of Health's Guide for the care and Use of Laboratory Animals. Monkey B was implanted with a Gray Matter 96 channel micro-drive system (GMA; Gray Matter Research) on the left hemisphere (Figure 2.1C). The GMA consists of micro-drive chamber, retainer, screw guide, and actuator with 96 electrodes. Each individual electrode could be advanced/retracted using a precision screwdriver up to 32 mm deep (125 μm/turn; 1.5 mm inter-electrode distance). The GMA was placed above the central sulcus targeting arm and hand area of both M1 and S1. The location of the central sulcus was determined based on the data from a structural MRI scan prior to surgical implantation. Accordingly, the GMA electrode tips probed caudal M1 and area 3a by canvassing the fundus and banks of the central sulcus. Monkey J was chronically implanted with two 64-electrode Utah microelectrode arrays (400 μm inter-electrode distance, 1.0 mm electrode length; Blackrock Microsystems, Salt Lake City, UT) in the hand area of M1 and S1 in the right hemisphere (Figure 2.1D). The location of the hand area of M1 was determined by evoking hand

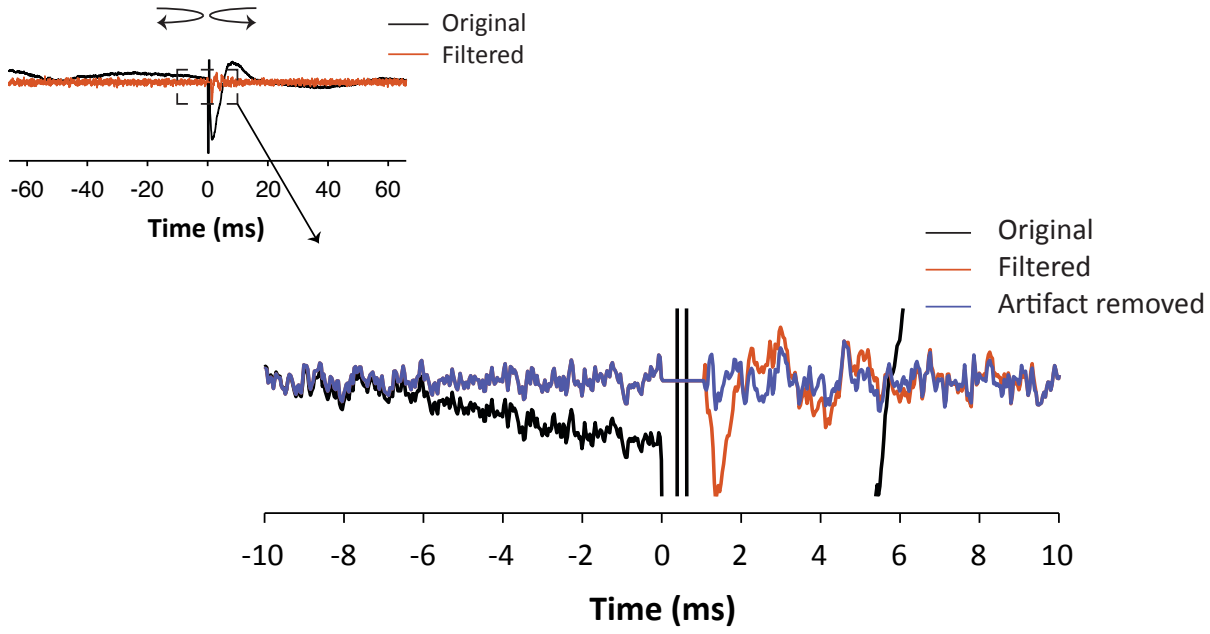

Figure 2. 2. Artifact removal process
Artifact removal has been done in 2 steps. First, we applied the high pass filter (300-6000 Hz) to the raw signal (black) to obtain filtered signal (red). Then, we fitted the filtered signal with Fourier series and subtracted it from the filtered signal to obtain artifact free signal (blue).

movements using surface electrical stimulation at the time of the surgery. The location of the hand area of S1 was estimated by referencing the lateral termination of the intraparietal sulcus.

Amplified neural signals (gain of 5000) were bandpass filtered between 0.3 Hz and 7.5 kHz and sampled at 30 kHz using the Cerebus Neural Data Acquisition system (Blackrock Microsystems, Salt Lake City, UT). Collected neural data were saved for further offline data analysis.

Intracortical microstimulation: To investigate the stimulation-evoked activity in both M1 and S1, we delivered electrical current pulses through selected electrodes while responses were recorded from all other electrodes. Stimulation currents were generated by a 96-channel programmable stimulator (Cerestim96, Blackrock Microsystems). Each pulse was configured as a biphasic pulse

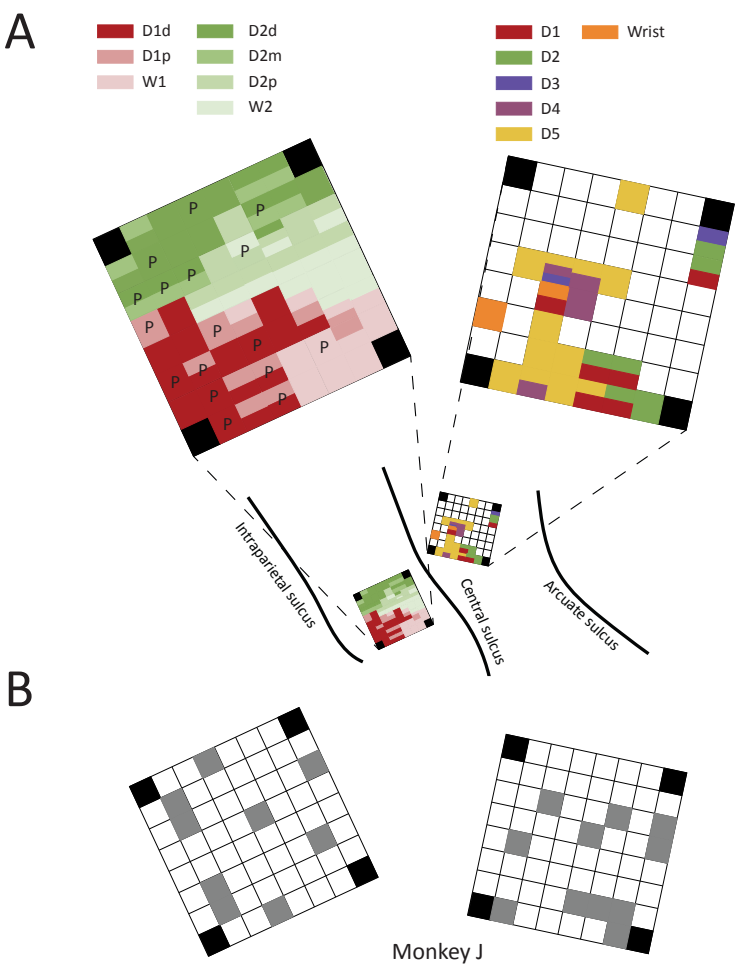

Figure 2. 3. Receptive field and projection field of M1 and S1 sites in monkey J

(A) Map of ICMS effects evoked at each electrode of array in S1 (left) and M1 (right). For S1 array, sites marked "P" showed proprioceptive response to the passive stimulation (i.e. stimulating on deep receptor or joint manipulation). (B) Gray colored sites were used for stimulation across all sessions. 9 and 11 sites were stimulated for S1 and M1 respectively.

(a 100 µs cathodic pulse followed by a 100 µs anodic pulse and a 100 µs inter-phase duration) with an amplitude of 30 µA. We used a continuous train of stimulation pulses at 10 Hz for both monkeys for the stimulation sequence (Figure 2.1B). Stimulation in M1 sites did not evoke any upper limb movement nor did it perturb the subject's grasping behavior. During each trial, ICMS onset time was precisely programmed that it was triggered when the robotic arm started to move to present the object to the animal. For monkey B, the stimulation duration was 1 sec, which spanned a period from the presentation of the object to approximately after monkey's hand began moving to grasp. For monkey J, the stimulation duration was expanded to 3 sec. It usually spanned the whole behavior epoch up to retraction of robotic arm. On each ICMS session, we pre-selected two sites (one M1 and one S1) on which to stimulate and stimulated for 100 consecutive trials per site. Upon completion of the behavior task session, we also stimulated the same electrodes while the monkey was at rest in its chair without

movement. While one experimenter was operating the stimulation software, another experimenter stayed in front of the monkey subject holding the reward which ensuring the animals remained in the preparatory posture (putting both arms on the arm rest).

Artifact reduction in the signals: During stimulation, a large and long stimulation artifact was observed on the other electrodes in the same bank and in the immediately adjacent banks (Figure 2.2, inset). Such artifacts greatly hindered our ability to identify a single neuron spiking within the duration of stimulation artifact. We took three steps routinely to reduce the stimulation artifact in the data collected from recording channels. Firstly, we used four 32 channels stimulation head-stages (Blackrock Stim Head-stage, Blackrock Microsystems). With this device, individual electrode channel can be used for both stimulation and recording simultaneously as it provides separate paths for stimulation and recording on the same probe. During the stimulation event, the stimulator has a direct path to the probe (electrode) and current does not go through the recording path because of the capacitor on its pathway to the recording device making the recording path act as an open circuit for the current coming from the stimulator. Second, we bi-directionally applied a high frequency band-pass filter (4^{th} order Butterworth, 300-6000 Hz) immediately before stimulation onset and after the stimulation offset to the raw continuous data (30 kHz sampling rate) (Figure 2.2, left-top). After we applied this filter to the signal on the recording channel, we replaced the stimulation artifact during the stimulation period (~500 μs) with a straight line that started with stimulation onset signal level and ended with stimulation offset signal level (blanking). Third, in cases where stimulation and recording channels were in the same bank, a secondary artifact was observed from the neural signal in the recording channel, which lasted ~6 ms on average. Since it contained a diminishing amplitude and increasing period in time, we fitted a 6^{th} order Fourier series

and subtracted it from the original signal to obtain an artifact-free signal (Figure 2.2, right-bottom). This signal then was saved and the single unit activity (spiking) was sorted using Offline Sorter (Plexon Inc. Dallas, TX).

Mapping receptive and projection field of neurons in S1 and M1: For monkey B, we used passive skin stimulation and joint manipulation to map the receptive field of neurons in S1 and M1. For S1 neurons, an experimenter stimulated the hand and arm skin using a cotton swap (light touch, soft brushing, and light taps) and hand joint (displacement and limb manipulation in a specific direction) and heard the neural modulations through the speaker, generated by the neural data acquisition software (Cerebus Central Suite, Blackrock Microsystems, Salt Lake City, UT). To identify area 2 and 3a neurons and the location of their receptive fields, we mainly focused on neural modulations for stimulating deep receptors and joint displacement. We carefully located the receptive fields of neurons by immobilizing other joints and only passively manipulating the joint of interest. We started manipulating proximal arm joints (elbow and shoulder) immobilizing more distal joints (wrist and finger). Then, we moved on to the wrist joints immobilizing the proximal joints. Finally, we manipulated each digit while holding all other more proximal joints fixed. Joint manipulations were done in 5 possible directions (flexion, extension, abduction, adduction, and supination). Mapping the receptive field of M1 neurons was done in a similar fashion. At around the suspected border of M1 and area 3a, once we located the neuron, we further verified whether the observed neuron was M1 or area 3a neuron using two separate approaches. First, we used suprathreshold ICMS (25 biphasic pulses with rate of 300 Hz, amplitude of 30 and 40 μA, and 200 μs width for each phase) to see if such an acute stimulation protocol evoked upper limb joint movements. For an observed evoked movement, the exact location of the perturbed joint was not

considered as we were simply distinguishing M1 and S1 sites during this procedure. Secondly, we further confirmed the neural modulation for active joint movement. To examine the neural modulation for active movement, we handed one of the objects to the animal to grasp and focused the modulation before onset of the movement. For each neuron we located, information about the depth and horizontal location of the corresponding electrode were recorded for further unit/site verification using histology.

For monkey J, we used skin stimulation and passive joint manipulation (S1) and ICMS (M1) to map the somatotopic organization of the cortical sites on which we implanted the electrode arrays (Figure 2.3A). S1 mapping in this procedure was similar to how we performed mapping on monkey B. For M1, we used high frequency, biphasic pulse stimulation protocol in an attempt to evoke upper limb movements to map the projection field of that site. Trains of 25 bi-phasic pulses were delivered at a rate of 300 Hz with 200 μs width for each phase. We carefully identified the exact location of muscle flexion and extension by palpating subject's upper limb muscles. One experimenter palpated proximal joint muscle first and moved toward distal joint muscle while another experimenter operated the stimulation software. We started at a high amplitude current of 100 μA and gradually decreased the amplitude down to 10 μA in steps of 10 μA. If there was no apparent movement evoked at the highest intensity, the electrode was considered unresponsive. We distinguished between movements evoked at the digits by palpation and visual inspection of the hand during ICMS and produced a map of ICMS effects for each array.

Histological process: Monkey B subject was transcardially perfused upon completion of the recording with 10% paraformaldehyde in saline. During perfusion, the electrodes were still located in the brain to easily visualize them. After we retracted the electrodes, we removed the brain from

the skull and soaked it in 30% sucrose phosphate buffer (PB). The section was then sliced with a cryostat in 60 micron slices, then stained every 6^{th} slice for VGlut2, Nissl, and Cytochrom Oxidase. We drew borders around area 3a using cytoarchitectonic markers. The caudal border of area 3a with 3b was identified after observing layer 4 becoming denser. The rostral border of area 3a with area 4 (M1) was identified where layer 4 dissipated almost completely and pyramidal cells in layer 5 became more prominent and evenly spaced. Histological borders were then registered to block-based images and electrode tracks were then labeled in those images to identify which ones passed through area 3a. Electrolytic lesions were also placed at strategic locations to ensure all electrode tracks could be reconstructed and localized.

Spatiotemporal properties of evoked responses to ICMS: To visualize the evoked effects of ICMS on other recording sites, we constructed peri-stimulus time histograms (PSTHs) of spiking with respect to the onset of the ICMS to analyze spatiotemporal properties of responses to ICMS. The time bin size used to construct PSTH was 0.3 ms. We followed Kraskov et al. and their criteria to identify the significant evoked responses (Kraskov et al., 2011): the post-stimulus response was considered as excitatory when at least three consecutive bins (1 ms) were above the mean + 2*SD and as inhibitory when at least five consecutive bins (1.5 ms) were below the mean – 1*SD. The

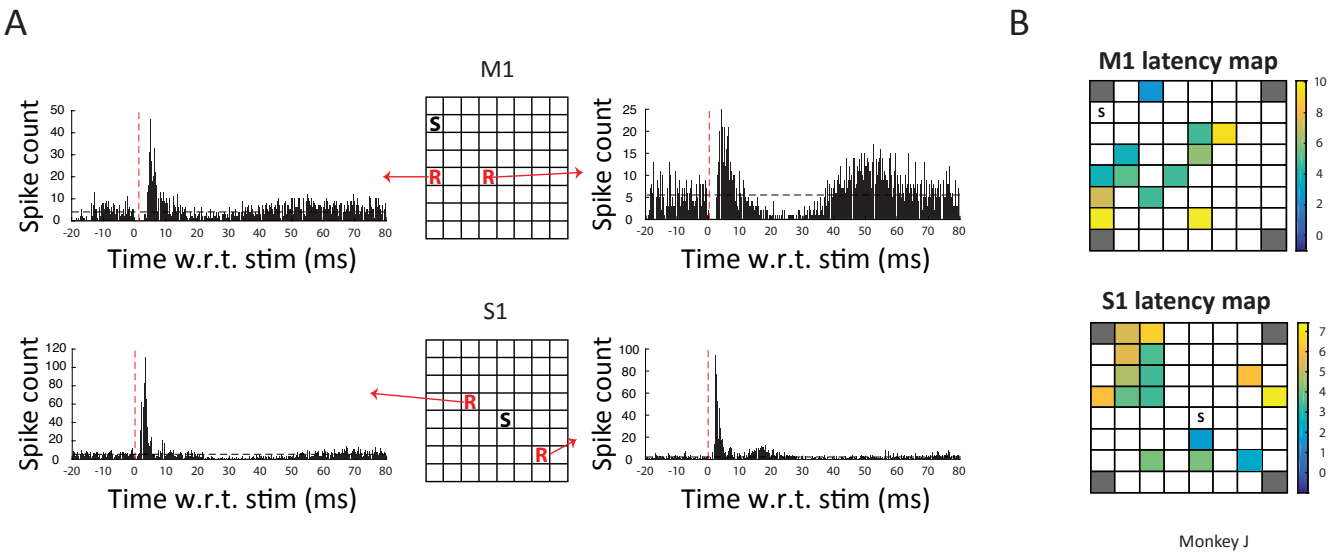

Figure 2. 4. Excitatory response within area

(A) Example excitatory response of single unit activity described using PSTH and recorded from the site labeled "R" (red) when the stimulation site "S" (black) is stimulated. Red dotted line indicates the stimulation onset time. M1 array (up) and S1 array (below) are plotted separately. (B) Response latency map from various recording sites. Response latency is defined as the time of excitatory peak in the PSTH since the stimulation onset.

mean and SD (standard deviation) of spiking of a given neuron in the response channel was evaluated on the PSTH 20 ms before the onset of ICMS. The response latency for the excitatory connection was estimated as the time from stimulation onset to the peak PSTH response. The strength of an excitatory response was measured as the peak PSTH value divided by the mean response.

Estimation of inter-electrode distance across areas (i.e. between M1 and S1 sites) was done considering the fundus of the central sulcus (CS). The depth of the CS was identified using an MRI image taken for array implantation (13 mm for monkey B and 14 mm for monkey J). Since it is impossible to measure the exact length of the cortical path between electrodes across area, we used the sum of Euclidean distance between each electrode and the bottom of the fundus for inter-electrode distance estimation.

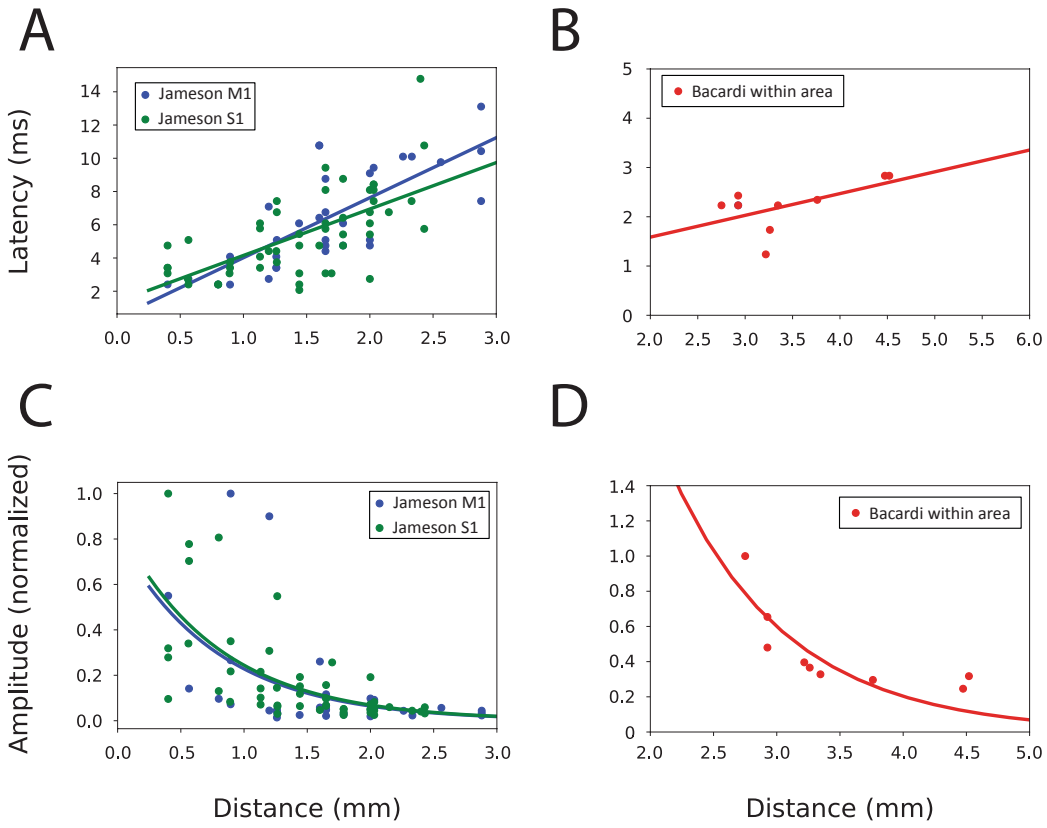

Figure 2. 5. Single neuron response to ICMS within area

(A,B) Relationship between inter-electrode distance (stimulating site and recording site) and single unit response latency recorded in the recording site in (A) monkey J and (B) monkey B. (C,D) Relationship between inter-electrode distance and single unit response amplitude in (C) monkey J and (D) monkey B.

Results

A total of 23 sessions (i.e. data sets) were collected and analyzed from 2 monkeys (10 sessions from monkey B and 13 sessions from monkey J). For each session per stimulating electrode, at least 35 trials of each object were presented (total of at least 210 trials/session). For monkey B, on a given day and before collecting data, we advanced or retracted all electrodes of the GMA in an attempt to search for clearly isolated single units. Among the identified units, across all monkey B sessions, we stimulated two area 3a sites, two area 2 sites, and six M1 sites. For monkey J, we

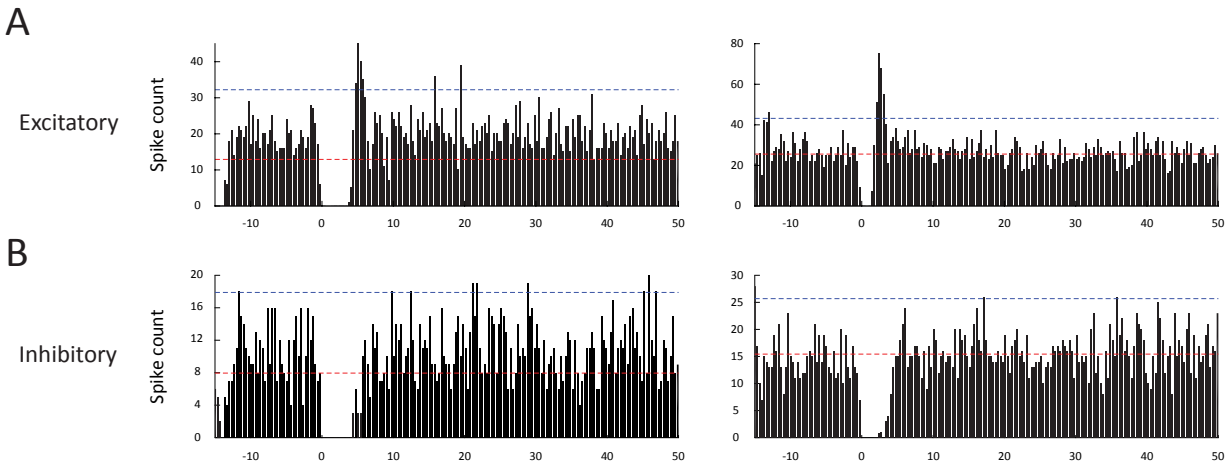

Figure 2. 6. Types of ICMS evoked responses across area

Average spike count is plotted in red and average spike count plus 2 times of its standard deviation is plotted in blue. (A) Excitatory responses and (B) inhibitory responses. Left column is the response of neurons in M1 for stimulating sites in S1. Right column is the response of neurons in S1 for stimulating sites in M1.

stimulated nine S1 and eleven M1 sites (Figure 2.3B). Clear isolation of single neuron activity in the recording channels was also required to investigate the causal interaction with stimulating channel.

For each monkey, 3 objects were pre-selected; a large cylinder out, a horizontal orientation of a large ring, and a large disk object for monkey B, and a large cylinder out, a vertical orientation of a large ring, and a vertical orientation of a small block for monkey J. These objects were selected because each monkey showed the most distinctive grasping behaviors with their hand using a K-nearest neighbor clustering algorithm on previously collected joint kinematic data.

In monkey J, two Utah electrode arrays (UEAs) were implanted in S1 and M1, one in each area. Projection field mapping of cortical sites in M1 using suprathreshold ICMS revealed that our implantation location covered many D1, D2, and D5 sites, and some of D3 and D4 sites (Figure 2.3A). With the range of ICMS intensity (10~100 μA), we failed to evoke any proximal limb movements. On the other hand, the UEA in S1 was implanted in the D1 and D2 representation sites, as well as proximal D2 (W2) and D1 (W1 and Thenar) based on manual hand mapping.

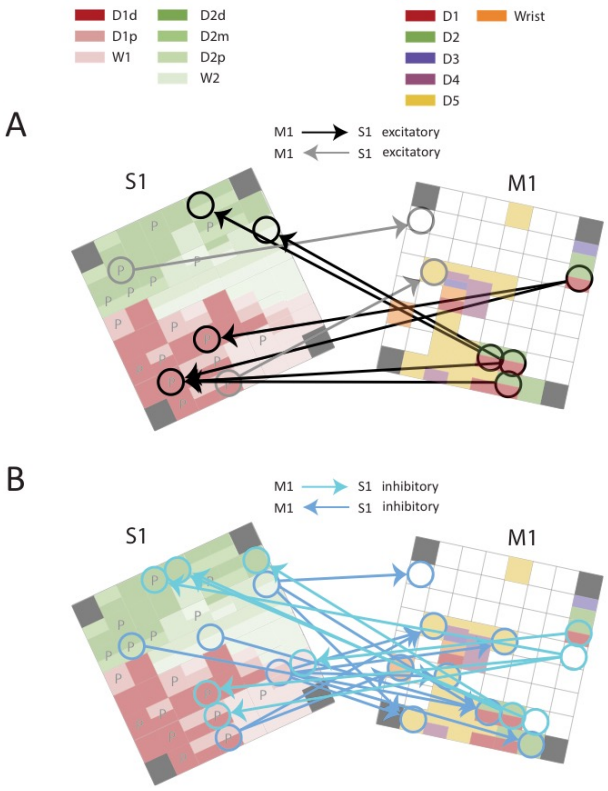

Figure 2. 7. Stimulation evoked responses across area
(A) Excitatory response evoked in S1 by stimulating M1 (black) and excitatory response evoked in M1 by stimulating S1 (gray). (B) Inhibitory response evoked in S1 by stimulating M1 (light blue) and inhibitory response evoked in M1 by stimulating S1 (dark blue).

Many neurons in the posterior side of the array showed modulations to passive joint displacement and deep receptor manipulation (Figure 2.3A), which indicates that this array was implanted on the border of area 1 and 2. In monkey B, since the size of the GMA was large enough to cover the entire M1 and S1 and individual electrode could be driven up to 32 mm, we could sample signals from many neurons and their receptive fields represented the whole hand. Ironically, however, due to its size and the inter-electrode distance, we could sample limited number of neural signals and the neural signal is much less stable, comparing to UEA setup.

ICMS response within area: Significant excitatory connections within area in both M1 and S1 were observed. Figure 4 shows typical excitatory connections between sites on the same array, using the single unit activity from the response electrodes. An excitatory peak was visually prominent for all excitatory connection pairs. In many cases with an excitatory connection, a

fluctuation of response followed initial excitatory peak (i.e. a prolonged suppression of single unit activity following the initial peak and then a secondary peak). The secondary peaks were usually smaller in amplitude, but could last as much as the first peak. Such secondary excitatory peaks, however, seemingly disappeared as the inter-electrode distance increased.

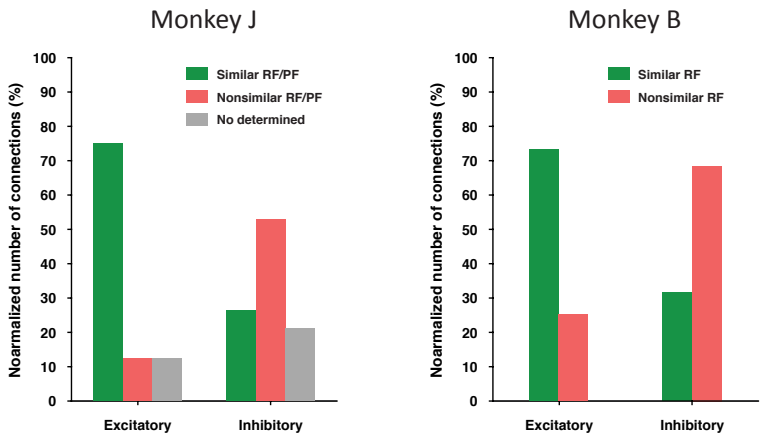

Figure 2. 8. Somatotopically organized corticocortical connection

Proportion of connections with RF/PF similarity in terms of sign of evoked response.

To examine spatiotemporal dynamics of response spread within the area, we measured the excitatory response latency from the sites from which we could sample single unit activity. Response latency is defined as the time duration between the stimulation onset and the initial excitatory peak. In monkey J, excitatory responses were observed between 2 to 10 ms after the stimulation onset, and the latency became shorter when the recording electrode was closer to the stimulating electrode. Figure 2.4B shows the sparse latency map for both M1 and S1 areas when the stimulating electrode (indicated as S) was stimulated. Although it is sparse due to the small number of recorded single units in both areas, an increasing latency can be seen with increasing distance between the stimulating and recording electrode. The speed of propagation of excitatory response, or conduction velocity assuming synaptic excitation, is estimated using information about the response latency and inter-electrode distance. Immediately adjacent electrode distance in our setup was 400 μm. We linearly regressed the response latency against inter-electrode distance for both arrays (Figure 2.5A). Conduction velocity was measured as a 1/slope of the above

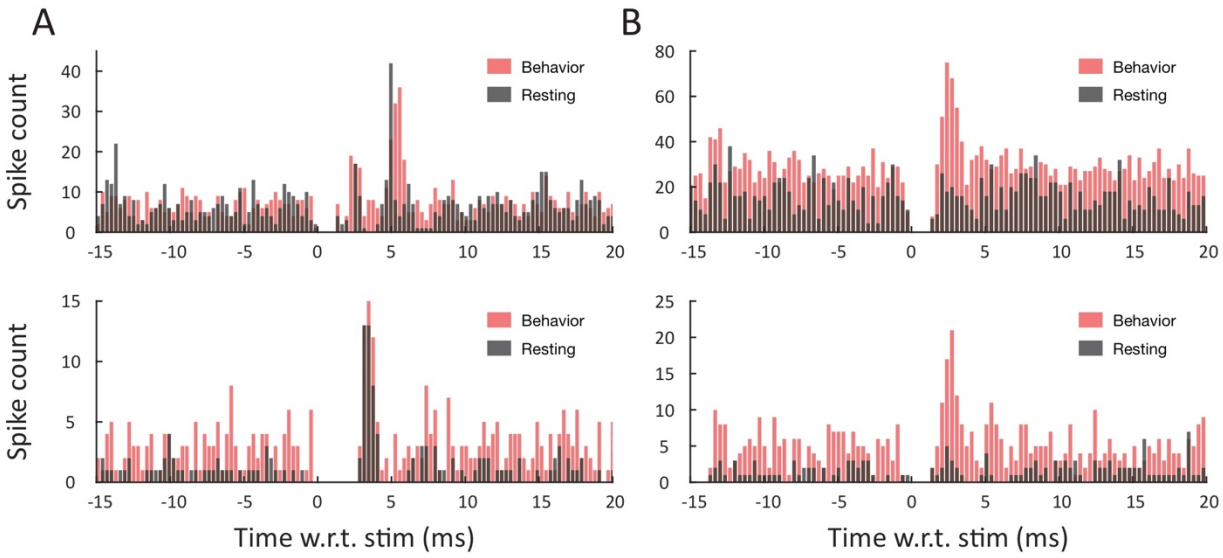

Figure 2. 9. Context dependent significant connection
(A) Example static significant excitatory connections between M1 and S1. Both PSTHs during the trial (red) and resting state (black) show significant connections. (B) Example of significant connections that change its mode in terms of behavioral state.

regression. Estimated conduction velocity in M1 and S1 for monkey J were 0.27 m/s and 0.35 m/s, respectively.

In monkey B, fewer number of single unit activity was sampled than monkey J as GMA has larger inter-electrode distance (1.5 mm) and signal itself is less stable than chronically implanted electrode recording setup. Nevertheless, we observed linear increment of latency with respect to the inter-electrode distance. The conduction velocity measured from the slope of regression line (Figure 2.5B, within area) for monkey B was 1.66 m/s.

The strength of connection is also measured by diving the peak excitatory value in PSTH divided by the average value of single unit activity which is measured the mean PSTH value in the time range of 20 ms before stimulation onset and stimulation onset time. Based on the visual inspection on PSTHs, exponential peak becomes less obvious and prominent as inter-electrode distance between stimulating and recording electrode becomes large. Excitatory response amplitude with respect to the inter-electrode distance is described in Figure 2.5C and Figure 2.5D.

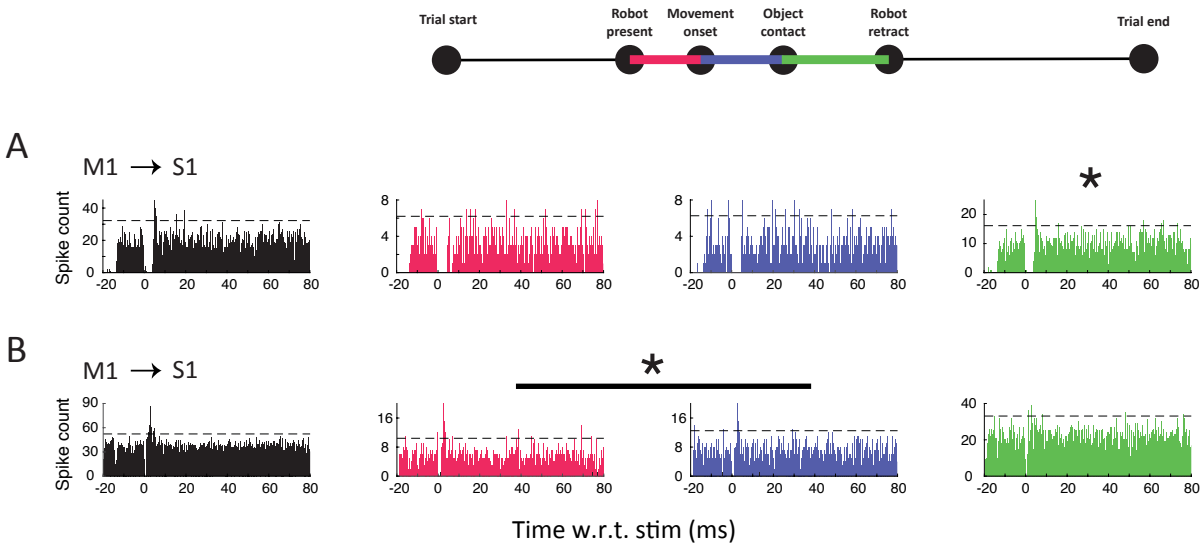

Figure 2. 10. State of connections changes depends on behavioral state
3 different states of grasping behavior were considered: between robot present and finger movement onset (red), between movement onset and object contact (blue), and between object contact and robot retract (green). (A) In this example excitatory pair (stim channel: M1 and recording channel: S1), when the PSTH during the grasping behavior (black) is separated into 3 different behavioral epochs, excitatory connection started to appear after the subject made contact with the object. (B) In this another example excitatory pair (stim channel: M1 and recording channel: S1), when the PSTH during the grasping behavior (black) is separated into 3 different behavioral epochs, excitatory connection started to disappear after the subject made contact with the object.

We regressed the amplitude against to the distance using an exponential function. In monkey J, the measured space constants for M1 and S1 were 1.264 mm and 1.265 mm, respectively. In monkey B, the measured space constant was 1.082 mm.

ICMS responses across area: To investigate cortico-cortical interactions between M1 and S1 sites during the grasp, we investigated PSTHs when the stimulating and recording electrodes were located in different areas.592 pairs (310 M1 stim-S1 rec pairs and 282 S1 stim-M1 rec pairs) were investigated in monkey J, and 87 pairs (33 M1 stim-S1 rec pairs and 54 S1 stim-M1 rec pairs) were investigated in monkey B. Across both monkeys and sessions, we observed bi-directional excitatory connections between M1 and S1 (Figure 2.6A).

Excitatory response across area: In monkey J, 4 out of 11 M1 sites we stimulated evoked excitatory response on some recording sites in S1 and 2 out of 10 S1 sites we stimulated evoked excitatory responses on some recording sites in M1 (Figure 2.7A). From our small sample of excitatory responses, a 1-to-1 excitatory connection was most frequent (i.e. a single stimulation site evoked an excitatory response on one single recording site). However, there were two M1 sites that each evoked excitatory responses on two separate S1 sites simultaneously. The average latency of excitatory responses across areas was 5.27 ± 0.76 ms. Linear fitting of the response latency against the inter-electrode distance showed that the conduction velocity of excitatory responses was 3.27 m/s. We used the three points linear distance estimation, bottom of fundus of CS being the middle point, to measure the inter-electrode distance. As this estimation assumes a straight line, the distance measure we used most likely is a lower bound of the actual distance across areas through the cortical tissue.

The analysis of monkey B's data was much more difficult to generalize due to the fewer number of neuron samples that were collected and the fact that we targeted multiple sub-regions of S1. In monkey B, 1 out of 6 M1 sites we stimulated evoked excitatory responses on some recording sites in S1, and 4 out of 8 S1 sites we stimulated evoked excitatory responses on some recording sites in M1. One site in area 3a evoked excitatory responses on two different sites in caudal part of M1 (cM1) and one site in the rostral part of M1 (rM1) received excitatory responses from two separate sites of 3a. The average latency of excitatory responses across areas was 3.04 ± 0.91 ms, and the conduction velocity of excitatory responses was 3.46 m/s.

Inhibitory response across areas: We observed not only significant excitatory connections across areas, but also inhibitory responses in both monkey subjects. An inhibitory response was characterized as a prolonged suppression of single unit activity without a peak on the recording site PSTH beginning at least 1.5 ms after onset of the stimulation (Kraskov et al., 2011). Reciprocal inhibitory connections were observed and were much more frequent than excitatory connections in both subjects. In monkey J, 4 out of 11 M1 sites we stimulated evoked inhibitory responses on some recording sites in S1, and 5 out of 10 S1 sites we stimulated evoked inhibitory responses on some recording sites in M1 (Figure 2.7B). Inhibitory connections in either direction was much more diverse than excitatory connections in that some stimulating sites resulted in inhibitory responses on multiple sites of another area simultaneously. The average duration of inhibitory suppression was 5.636 ± 2.521 ms. In monkey B, 4 out of 6 M1 sites we stimulated evoked inhibitory response on some recording sites in S1 and 4 out of 8 S1 sites we stimulated evoked inhibitory responses on some recording sites in M1. The average duration of inhibitory suppression was 3.07 ± 0.714 ms. Again, inhibitory connections across sub-region of M1 (rM1 and cM1) and S1 (area 3a and 2) were more frequently observed and diverse than excitatory connections. However, in both monkeys, further analysis on inhibitory responses revealed no apparent structure in the relationship between inter-electrode distance and suppression duration or directionality of inhibitory responses across areas.

Relationship between cortico-cortical connections and somatotopy: To investigate the relationship between the sign of the cortical connection (excitatory vs. inhibitory) across areas and the somatotopic organization of the paired sites, we directly compared significant connections and each neuron's receptive field (RF in S1) or projection fields (PF in M1) organization. In monkey

J, a total of 21 M1 sites out of 60 were selected for the current analysis because we could isolate clear neural signal from only a subset of M1 electrodes and not all electrodes with recorded single units evoked upper limb movement when suprathreshold ICMS was used. Fortunately, we observed diverse digit projection field distributions in M1 site and D1/D2 receptive field representations in S1 (Figure 2.3A). We found a positive relationship between excitatory connection responses and their RF/PFRF representations. 8/21 studied M1 sites showed at least partial PF representations of either D1/D2 and when stimulated, 4 sites out of those 8 sites evoked excitatory responses on some sites in S1. On the other hand, no single site in M1 with PF representations of other joints, such as D3, D4, D5, or wrist evoked excitatory responses in S1. Only one exception was observed when stimulating one S1 site with D1p and thenar RF representations evoked an excitatory response on one M1 site with a D5 PF representation. One pair (S1 stim-M1 rec) could not be determined for this analysis because the target M1 site did not evoke movements with the highest ICMS current levels used. To summarize, 6 out of 8 observed excitatory connections across areas were from the pairs with similar RF/PF representations. 1 out of 8 was from dissimilar RF/PF representations, although their RF/PF representations partially overlapped, and 1 out of 8 could not be determined (Figure 2.8). In monkey B, the results marginally agreed with the results we observed in monkey J. 4 out of 6 observed excitatory connections were from pairs with similar RF/PF representations (Figure 2.8).

In the case of inhibitory connections, many dissimilar RF/PF organization pairs were recruited. For example, in monkey J, we found 13 M1 sites that evoked movements in D3, D4, D5, or wrist joint. Of these 13 sites, 5 sites showed evoked inhibitory responses for stimulating S1 sites with D1 or D2 site RF representations. None of those M1 sites showed excitatory responses in the previous analysis. Among pairs with similar RF/PF across areas, they are all from stimulating M1

sites (2 out of 8 D1/D2 sites showed such examples). To summarize, 12 out of 18 observed inhibitory connections across area were from pairs with dissimilar RF/PF representations. 3 out of 18 were from similar RF/PF representations and 4 out of 18 could not be determined (Figure 2.8). For monkey B, the result showed similar tendencies. 16 out of 20 observed inhibitory connections across areas were from pairs with dissimilar RF/PF representations and the remaining 4 were from similar RF/PF representations (Figure 2.8).

Context-dependent connections across areas: We investigated whether these functional cortical connections depended on the behavioral state of the animal. In a given session day, upon completion of behavioral task, we stimulated while the subject was resting in its chair. The same electrodes were stimulated during this period, and since monkey's head was restrained for the whole time, we were most likely stimulating and recording the same units from the behavioral task. The state of sensorimotor cortical neurons during the resting period was generally characterized by lower firing rates without apparent modulation. Some excitatory connection pairs across areas in both monkeys didn't show significant change in the resting versus task states, although weaker overall spiking activity was apparent (Figure 2.9A). However, a sizable number of excitatory connections across areas showed significant differences. Figure 2.9B shows example excitatory connections responses during the task state that disappeared during the resting state. In monkey B, 4 out of 6 excitatory connections and in monkey J, 3 out of 8 excitatory connections showed such differences.

Having established the fact that the connections between M1 and S1 are plastic and state-dependent, we further analyzed their connectivity state in a different behavioral epoch of the grasping task. In one monkey subject (monkey J), stimulation lasted for 3 second from the onset

of the stimulation which was locked to the object presentation of the robot arm which spanned, on average, up to 0.5 second after robot arm retraction. We separated the behavior into three epochs: 1) between object presentation and subject hand movement onset (BOPMO), 2) between subject hand movement onset and object contact (BMOOC), and 3) between object contact and robot arm retract (BOCRR) (Figure 2.10). PSTHs in the 3 different behavioral epochs were constructed and compared to analyze context dependency of excitatory connections.

We found two types of context-dependent connectivity. Some excitatory connections (3/8) didn't show evidence of excitatory connections during the first two behavioral epochs (BOPMO and BMOOC), but an excitatory peak started to appear after the subject made contact with the object (Figure 2.10A). Although neural modulation of object contact may have resulted in an increasing total number of spikes in different behavioral epochs, a peak in the stimulation triggered PSTH is a prominent feature of causal effect of excitatory connections. The second type of context-dependent connectivity showed exactly the opposite results to the first type (Figure 2.10B). For some excitatory connections (2/8), evoked excitatory connections were observed during the first two behavioral epochs (BOPMO and BMOOC), but the excitatory peak vanished after the subject made contact with the object.

Discussion

We used a combination of multi-electrode arrays and ICMS techniques to investigate spatiotemporal structure of functional connectivity between neurons in M1 and S1 during a hand grasping task. This study provided three important results. First, low-intensity ICMS pulses directly applied to sites either in M1 or S1 hand area provided evidence for reciprocal excitatory

and inhibitory functional connections across both areas. Second and more importantly, such connections were organized in non-random fashion such that those pairs with excitatory connections were more likely to share similar receptive/projection fields. Likewise, pairs with inhibitory connections were more likely to have dissimilar receptive/projection fields. This provides causal evidence for our overarching hypothesis that functional connectivity is organized somatotopically. Third, connections across M1 and S1 are context-dependent that upper limb behavioral state alters their functional connections suggesting that these functional connections do not purely reflect rigid anatomical connectivity.

Simultaneous stimulating and recording: Since the early days of neuroscience, electrical stimulation within the brain has been a main tool for examining brain function (Fritsch and Hitzig, 1870). ICMS has been popular technique for mapping the function of small populations of cortical neurons (Asanuma and Rosen, 1972; Asanuma et al., 1973; Cheney et al., 1985; Nudo et al., 1996; Baker et al., 1997; Park et al., 2001; Jackson et al., 2006; Hao et al., 2016) and their synaptic connectivity with other cortical areas (Asanuma et al., 1968; Rosen and Asanuma, 1972; Asanuma et al., 1982; Mori et al., 1989; Kraskov et al., 2011). Recent developments in state-of-the-art multi-site stimulating and recording systems have enabled us to conduct extremely fast and yet, stable ICMS experiments. In this study, we reliably and simultaneously stimulated and sampled single neural activity from multiple recording sites despite the existence of stimulation artifact originating from capacitive coupling between stimulating and recording electrodes (McGill et al., 1982). Use of switch-less stimulation head stages and potentiometers enabled us to record high frequency signals within 1 ms after stimulus offset without possibility of high level of stimulation current flowing into the recording amplifier due to the capacitive coupling.

ICMS response characteristics: within area: Previous studies (Kraskov et al., 2011; Hao et al., 2016) as well as our data show the typical characteristics of evoked excitatory responses due to ICMS: a short peak (1~3 ms) of single unit activity followed by a much longer duration of suppression (~20 ms). Interestingly, the suppression that follows after the initial excitatory peak in M1 is even longer while the animal was in the resting state (~50 ms). Such excitatory responses are thought to be driven by synaptic projections from the neuron and axons located close to the stimulating electrode in the form of transsynaptic activation (Kraskov et al, 2011). Previous ICMS studies in primates M1 (Hao et al., 2016) suggested such the long suppressive effects are due to a cascade of oligosynaptic effects on the local inhibitory network which in turn, affects neurons on the recording site. The inhibitory effects that followed the excitatory peaks in our data (monkey J), however, showed much longer durations (Figure 2.4) than previous study reported (Hao et al., 2016, ~10 ms). This discrepancy may be due to the fact that our UEA electrode length was 1.0 mm which is targeting superficial cortical layers (likely layers 2/3) and that cortical network is differently recruited. Given that GABA interneurons in the monkey sensory-motor cortex are most concentrated in the layer 2-4 (Houser et al., 1983), it is likely we stimulated a greater population of inhibitory network which resulted in longer duration suppression.

Spatiotemporal dynamics of excitatory connectivity within an area was also measured. Computed conduction velocity in each area as 1/slope of the linear regression of latency vs. distance, agreed with the propagation velocity of traveling waves within the cortex of awake monkeys (Rubino et al., 2006; Nauhaus et al., 2009; Muller et al., 2014; Takahashi et al., 2015). The space constant measured by the exponential fit of excitatory response amplitude versus distance also matched M1 data from Hao et al. and visual cortex data (Nauhaus et al., 2009).

ICMS response characteristics: across areas: It is natural to hypothesize that there should exist significant functional connectivity between M1 and S1 considering their close proximity and similarity in topographical organizations. Indeed, their direct connections have been studied in mice (Ferezou et al., 2007), cats (Sakamoto et al., 1987; Sakamoto et al., 1989), monkeys (Jones et al., 1978; Pavlides et al., 1993; Schmahmann and Pandya, 2006), and human (Conturo et al., 1999; Shinoura et al., 2005; Guevara et al., 2011; Catani et al., 2012). Catani and colleagues showed the existence of associative fibers (also called U-fiber) between precentral and postcentral gyrus in human (Catani et al., 2012) using spherical deconvolution diffusion tractography technique. The volume and number of U-fiber in the hand area is the greatest among other areas they investigated (proximal arm, mouth, and foot) supporting the idea that stronger communication in necessary in areas that require finely tuned movement and complex motor skills.

We found reciprocal connectivity between M1 and S1 in this study. A major source of corticocortical projections is known to originate in layer 3 (lamina III pyramids) (Jones and Wise, 1977; Douglas and Martin, 2004) and our electrodes in monkey J presumably were targeting layer 3 and 4. However, the number of connections between M1 and area 2 we found was surprisingly sparse: only 8 excitatory connections and 19 inhibitory connections out of 592 pairs were found in monkey J. Conduction velocities between areas in both monkeys were consistent with those found among myelinated neurons (conduction velocity: 3.27 m/s in monkey J and 3.46 m/s in monkey B) whose axons travel through association fibers between precentral gyrus (motor area) and postcentral gyrus (somatosensory area) (Guevara et al., 2011; Catani et al., 2012).

In monkey J, we found three times as many excitatory responses in S1 evoked by stimulating M1 than responses in M1 evoked by stimulating S1. This finding is in line with two other previous studies about the function of corticocortical somatosensory input to the motor cortex,

which is closely tied with motor learning. Sakamoto and his colleagues found that stimulation in somatosensory cortex induced long-term potentiation (LTP) in the motor cortex (Sakamoto et al., 1987). However, stimulation to the ventrolateral nucleus of the thalamus failed to induce LTP (Iriki et al., 1991). From these two experiments, sensory connections relayed through S1, as an indirect thalamo-somatosensory-motor route, induce LTP in the motor cortex that help to consolidate motor schemas and novel movement combinations. Indeed, a S1 lesion study showed that a monkey subject with S1 inactivation failed to learn a new motor skill but was able to perform skills that had been learnt previously (Pavlides et al., 1993). Both our monkey subjects had learned the grasping task for over 2 years before we began our experiments suggesting that motor skill learning was no longer taking place. This may be a main cause of lack of excitatory signal from S1 to M1 that we observed. In the case of inhibitory responses, we found twice as many inhibitory responses in M1 evoked by stimulating S1 than responses in S1 evoked by stimulating M1 (Figure 2.7). This is in line with the finding that U-fiber tracks represent an alternative indirect modulatory somatosensory-motor signal (Hikosaka et al., 1985).

Somatotopic association between M1 and S1: In the current model of visually guided hand grasping, connections between M1 and S1 are largely ignored or considered insignificant (Grafton, 2010). The very few studies that have investigated the connectivity structure between M1 and S1 in terms of their functional organization (Asanuma et al., 1968; Thompson et al., 1970; Asanuma et al., 1982; Herman et al., 1985) were conducted in the cat and have collectively found that connections between M1 and S1 are somatotopically organized. Our current study first confirmed somatotopically organized connectivity in awake monkey. We further found that the significant connections across areas are not hard-wired connections, but show great deal of context

dependence in terms of subject's behavioral state. At least two interpretations can be made about somatotopically organized dynamic connections. First, somatotopically matched connection may be formed as signals from somatosensory cortex projecting instructive signals necessary for motor learning. Evidence for this comes from a study that showed that the absence of direct somatosensory input to the motor cortex hindered learning a novel motor behaviors and recovery of motor function after removal of the tumor, and damage to the motor hand region was associated with increased activation of the somatosensory area (Shinoura et al., 2005). This result indicates that M1 neurons' functional properties are formed and guided by somatosensory input from S1 and somatotopically matched communication structure between them is inevitable. Second, functional communication structure between M1 and S1 may facilitate the synergistic coordination of movement with sensation. M1-S1 excitatory connection pairs that we found were recruited differently in terms of the subject's behavioral state (Figure 2.10), indicating rapid online feedback communication structure from M1 to S1 (i.e. efference copy or somatosensory prediction). Establishing functionally aligned connections between two areas is advantageous for efficient execution and control of the movement. Together, we conclude that functionally aligned connectiviy may play a significant role during motor learning from the beginning of learning any motor task (S1 to M1) to efficient execution (M1 to S1).

Discussion

The goal of this thesis can be concisely stated: how corticocortical communication between neurons in macaque M1 and S1 in hand area relate to their somatotopic organization? We designed and performed experiments to answer this question using two different approaches: statistical modeling and ICMS. Because I included a discussion section specific to each chapter, I will focus on establishing a general conclusion about this thesis in this final chapter.

In the current model of generation of visually guided hand grasping circuit, the significance of connectivity structure between the primary motor (M1) and somatosensory area (S1) is missing (Davare et al., 2011). More specifically, online somatosensory feedback is assumed to be provided only through long process of the original grasping circuit. However, the existence of direct anatomical connections between M1 and S1 (Jones et al., 1978; Conturo et al., 1999; Shinoura et al., 2005; Guevara et al., 2011; Catani et al., 2012) and corticomotoneuronal (CM) cells in S1 (partially in area 3a) lets us cast a serious question about the role of S1 in motor behavior, especially, with the current model of grasping. One might ask, why are somatotopically similar sites in M1 and S1 functionally connected? Our results suggest this co-registration of similar somatotopic fields between connected M1 and S1sites might be significant for online feedback similar to Asanuma's concept of the motor cortical column in which sites have projection and receptive fields that are co-registered to the same limb segment.

In chapter 2 of this thesis, we incorporated band pass filtered LFP and used this signal as a proxy of local population activity at a cortical site. The gamma band component of LFP was used in our study, which is thought to emerge from the coordinated interaction of excitation and inhibition (Buzsáki and Wang, 2014). In chapter 3, we found both excitatory and inhibitory reciprocal connections between M1 and S1 that might be mediated by gamma frequency band

synchronous neural activity. It is not clear, however, why theta band LFP (4~7 Hz) contains predictive power about neural activity across M1 and S1. Previous studies in the forelimb area of M1 and S1 found that theta synchrony is organized according to movement phases (Feige et al., 2000; Ohara et al., 2001). On the other hand, studies on hippocampal CA1 cells and orbitofrontal neurons found phase locking between neuronal firing and theta bandpass-filtered LFP during goal directed reward expectancy (Wingerden et al., 2010; Lansink et al., 2016). Considering our data involves a task consisting of a long period of time before movement execution, it is possible that the signal about the reward expectancy is incorporated in the interaction between target pairs of neurons in M1 and S1 of highly trained monkeys.

Our group has extensively investigated beta oscillations and their attenuation at movement initiation (Donoghue et al., 1998; O'Leary and Hatsopoulos, 2006; Rubino et al., 2006; Saleh et al., 2010; Reimer and Hatsopoulos, 2010; Takahashi et al., 2011). In the current study, we did not include the beta band component (15~30 Hz) of the LFP because its amplitude vanishes and becomes insignificant after movement initiation. However, we did observe high spike-field coherence in the beta frequency band before movement onset and after movement offset in both M1 and S1 spike-field pairs (data not shown).

Our group's previous work found that M1 encode complex temporal kinematics trajectories spanning multiple joints (Saleh et al., 2012). We observed similar findings in both M1 and S1 such that the response fields of single units in these areas were better predicted when temporally extended multiple joint kinematics were used as predictors. Relevant joint kinematics for a given neuron were selected using a feature importance algorithm (LASSO). One difference between Saleh et al.'s GLM approach and ours is that we did not include intrinsic spike history covariates. Naturally, it is advised to account for intrinsic effects of spiking history (e.g. refractory period or

Ca^{+2}/K ion based afterhyperpolarization suppression). However, in our study, we specifically focused on the influence of extrinsic kinematic features on spiking activity.

We used ICMS to investigate spatiotemporal and functional connectivity between M1 and S1. Prominent inhibitory connections between dissimilar joint representations of M1 and S1 were observed. This agrees with previous studies that found modulatory signals originating from S1 to M1 (Shinoura et al., 2005). Also, we found that excitatory connections were preferentially established between M1 and S1 sites with similar somatotopic representation sites. We suspect such connections serve specific functions in grasping behavior, such as facilitation of synergistic neural coding that is suspected to exist in early visual areas (Cleland et al., 1971; Mciiwain, 1973, 1977; Tanaka, 1983; Ts'o et al., 1986; Hata et al., 1991; Salin et al., 1992).

Future direction

In this thesis, we explored cortico-cortical connections between M1 and S1 and their somatotopic organization. According to the result that we presented in this thesis, we should consider the significance of S1 online modulatory signal to M1 and M1's online signal to the somatosensory cortex (i.e. efference copy or somatosensory prediction, see Adams et al., 2013 for review) in the motor control. Many current efforts to develop upper-limb actuated and sensorized neuroprostheses involve extracting and decoding signals from motor cortices to control an effector and stimulating somatossensory neurons to convey tactile feedback to the patient about the state of the prosthesis (Hatsopoulos and Donoghue., 2009). Endeavors to convey proprioceptive feedback through ICMS, however, are severely hindered by inadequacies in our understanding of how joint movements are encoded in the activity of populations of neurons in somatosensory

cortex. Therefore, understanding the functional communications between M1 and S1 not also addresses fundamental questions about the neural mechanisms of sensorimotor control, but also has important practical implications in the development of upper-limb neuroprostheses.

Although we observed considerable evidence of functional connections between M1 and S1 during the hand grasping, our work has raised questions that we have not yet answered. In the rest of discussion section, I would like to introduce a question that we raised during this study and an experiment to test the hypothesis.

Previous work on somatosensory input to M1 found that ICMS in sensory cortex induced long-term potentiation (LTP) in the motor cortex (Sakamoto et al., 1987). However, stimulation to the ventrolateral nucleus of the thalamus failed to induce LTP in motor cortex (Iriki et al., 1991). From these two experiments, sensory connections relayed through S1, as an indirect thalamo-somatosensory-motor route, induce LTP in the motor cortex that helps to consolidate motor schemas and novel movement combinations. Indeed, a S1 lesion study showed that a monkey with S1 inactivation failed to learn a new motor skill although was able to perform skills that had been learnt previously. Both our monkeys had learned the grasping task for more than 2 years prior to our experiments. We speculate that this explains why we observed relatively sparse connectivity from S1 to M1. To further establish the role of S1 to M1 connections in modulatory function, we would like to suggest the following experiment.

In this experiment, two awake behaving rhesus macaques would be trained in the grasping task. The first monkey (monkey A) would be trained to grasping 3 objects that display the most distinctive grasping postures. After the training, monkey A would be implanted with 1 Utah electrode array (UEA) in the somatosensory cortex and 1 UEA in the motor cortex on the contralateral side of the trained hand. As described in the chapter 3 of this thesis, monkey A would

perform the grasping task while we deliver subthreshold ICMS trains to one electrode of the either array and record the responses from all other electrodes. Another monkey (monkey C), however, would be naïve to the task or instructed to have very minimal exposure to the grasping task. We would implant UEAs into the same locations of the brain and deliver suthreshold ICMS trains while the monkey C is being trained for the task. Given that we have data from one monkey (monkey B in chapter 3) in this very ICMS experiment protocol, we would have 2 well-trained animals (monkeys A and B) to compare with 1 test animal (monkey C). In this way, we would be able to test if we could observe more functional connections from S1 to M1 in monkey C than in the other two completely trained animals (monkeys A and B).

Behaviorally, we would measure joint kinematics of monkey C as it is allowed. After mapping the receptive fields using hand mapping and projection fields using a suprathreshold ICMS protocol, we would decide which joint kinematics we would track. Given that monkey C is naïve to the task, it would likely display high variability in the joint kinematics as it tries different grasping strategies and learns the optimal movement for grasping. We would perform principal components analysis (PCA) on the multiple joint kinematics to derive the first several principal joint movements and see how these movement dynamics settled as training goes on.

On the other hand, assuming inhibitory connections from S1 to M1 are most prominent during the task learning period, we would expect fewer inhibitory signals from S1 to M1 upon completion of training. Then, we would relate motor learning to the evolution of inhibitory connections in sensorimotor cortical areas. If inhibitory connections of given pairs of neurons are indeed a signature of motor learning, the dynamics of signal quality and/or strength between sites should adopt as a monkey subject learn to the task. Comparison analysis of the motor learning and

inhibitory connections across area would shed a significant light on our understanding of M1-S1 interactions in the motor control.

References

Arce-McShane, Fritzie I., et al. "Primary motor and sensory cortical areas communicate via spatiotemporally coordinated networks at multiple frequencies." *Proceedings of the National Academy of Sciences* 113.18 (2016): 5083-5088.

Asanuma, H., S. D. Stoney Jr, and C. Abzug. "Relationship between afferent input and motor outflow in cat motorsensory cortex." *Journal of Neurophysiology* 31.5 (1968): 670-681.

Asanuma, H., R. S. Waters, and H. Yumiya. "Physiological properties of neurons projecting from area 3a to area 4 gamma of feline cerebral cortex." *Journal of neurophysiology*48.4 (1982): 1048-1057.

Asanuma, Hiroshi, and Ingmar Rosén. "Spread of mono-and polysynaptic connections within cat's motor cortex." *Experimental brain research* 16.5 (1973): 507-520.

Asanuma, Hj, and I. Rosen. "Topographical organization of cortical efferent zones projecting to distal forelimb muscles in the monkey." *Experimental brain research* 14.3 (1972): 243-256.

Baker, S. N., Etienne Olivier, and R. N. Lemon. "Coherent oscillations in monkey motor cortex and hand muscle EMG show task-dependent modulation." *The Journal of physiology*501.1 (1997): 225-241.

Bäumer, T., et al. "Inhibitory and facilitatory connectivity from ventral premotor to primary motor cortex in healthy humans at rest–a bifocal TMS study." *Clinical Neurophysiology* 120.9 (2009): 1724-1731.

Belitski, Andrei, et al. "Low-frequency local field potentials and spikes in primary visual cortex convey independent visual information." *Journal of Neuroscience* 28.22 (2008): 5696-5709.

Betz, W. "Anatomischer nachweis zweier gehirncentra." *Zentralbl Med Wiss* 12.578,595 (1874).

Blum, Baruch, Lawrence M. Halpern, and Arthur A. Ward Jr. "Microelectrode studies of the afferent connections and efferent projections of neurons in the sensorimotor cortex of the cat." *Experimental neurology* 20.1 (1968): 156-173.

Borra, Elena, et al. "Cortical connections of the macaque anterior intraparietal (AIP) area." *Cerebral Cortex* 18.5 (2007): 1094-1111.

Bragin, Anatol, et al. "Gamma (40-100 Hz) oscillation in the hippocampus of the behaving rat." *The Journal of Neuroscience* 15.1 (1995): 47-60.

Bremmer, Frank, et al. "Visual–vestibular interactive responses in the macaque ventral intraparietal area (VIP)." *European Journal of Neuroscience* 16.8 (2002): 1569-1586.

Burns, Samuel P., Dajun Xing, and Robert M. Shapley. "Comparisons of the dynamics of local field potential and multiunit activity signals in macaque visual cortex." *Journal of Neuroscience* 30.41 (2010): 13739-13749.

Buzsáki, György, Costas A. Anastassiou, and Christof Koch. "The origin of extracellular fields and currents—EEG, ECoG, LFP and spikes." *Nature reviews neuroscience* 13.6 (2012): 407-420.

Buzsáki, György, and Andreas Draguhn. "Neuronal oscillations in cortical networks." *science* 304.5679 (2004): 1926-1929.

Buzsáki, György, and Xiao-Jing Wang. "Mechanisms of gamma oscillations." *Annual review of neuroscience* 35 (2012): 203-225.

Cabel, D. William, Paul Cisek, and Stephen H. Scott. "Neural activity in primary motor cortex related to mechanical loads applied to the shoulder and elbow during a postural task." *Journal of neurophysiology* 86.4 (2001): 2102-2108.

Calabrese, Ana, et al. "A generalized linear model for estimating spectrotemporal receptive fields from responses to natural sounds." *PloS one* 6.1 (2011): e16104.

Churchland, Mark M., and Krishna V. Shenoy. "Temporal complexity and heterogeneity of single-neuron activity in premotor and motor cortex." *Journal of neurophysiology* 97.6 (2007): 4235-4257.

Cheney, PAUL D., EBERHARD E. Fetz, and SUZANNE SAWYER Palmer. "Patterns of facilitation and suppression of antagonist forelimb muscles from motor cortex sites in the awake monkey." *Journal of neurophysiology* 53.3 (1985): 805-820.

Cleland, B. G., M. W. Dubin, and W. R. Levick. "Simultaneous recording of input and output of lateral geniculate neurones." *Nature New Biology* 231.23 (1971): 191.

Cover, Thomas M., and Joy A. Thomas. *Elements of information theory*. John Wiley & Sons, 2012.

Crago, PATRICK E., JAMES C. Houk, and WILLIAM Z. Rymer. "Sampling of total muscle force by tendon organs." *Journal of neurophysiology* 47.6 (1982): 1069-1083.

Cui, Yuwei, et al. "Inferring cortical variability from local field potentials." *Journal of Neuroscience* 36.14 (2016): 4121-4135.

Cusick, C. G., D. A. Steindler, and J. H. Kaas. "Corticocortical and collateral thalamocortical connections of postcentral somatosensory cortical areas in squirrel monkeys: a double-labeling study with radiolabeled wheatgerm agglutinin and wheatgerm agglutinin conjugated to horseradish peroxidase." *Somatosensory research* 3.1 (1985): 1-31.

Delp, Scott L., et al. "OpenSim: open-source software to create and analyze dynamic simulations of movement." *IEEE transactions on biomedical engineering* 54.11 (2007): 1940-1950.

Divac, I., et al. "Heterogeneous afferents to the inferior parietal lobule of the rhesus monkey revealed by the retrograde transport method." *Brain research* 123.2 (1977): 197-207.

Dinopoulos, A. "Reciprocal connections of the motor neocortical area with the contralateral thalamus in the hedgehog (Erinaceus europaeus) brain." *European Journal of Neuroscience* 6.3 (1994): 374-380.

Donoghue, J. P., S. Leibovic, and J. N. Sanes. "Organization of the forelimb area in squirrel monkey motor cortex: representation of digit, wrist, and elbow muscles." *Experimental Brain Research* 89.1 (1992): 1-19.

Donoghue, John P., et al. "Neural discharge and local field potential oscillations in primate motor cortex during voluntary movements." *Journal of neurophysiology* 79.1 (1998): 159-173.

Duhamel, Jean-René, Carol L. Colby, and Michael E. Goldberg. "Ventral intraparietal area of the macaque: congruent visual and somatic response properties." *Journal of neurophysiology* 79.1 (1998): 126-136.

Edin, Benoni B. "Cutaneous afferents provide information about knee joint movements in humans." *The Journal of Physiology* 531.1 (2001): 289-297.

Einevoll, Gaute T., et al. "Modelling and analysis of local field potentials for studying the function of cortical circuits." *Nature Reviews Neuroscience* 14.11 (2013): 770.

Evarts, Edward V. "Relation of pyramidal tract activity to force exerted during voluntary movement." *Journal of neurophysiology* 31.1 (1968): 14-27.

Farkas, Tamás, et al. "Activation of the primary motor cortex by somatosensory stimulation in adult rats is mediated mainly by associational connections from the somatosensory cortex." *Neuroscience* 90.2 (1999): 353-361.

Feige, Bernd, A. D. Aertsen, and Rumyana Kristeva-Feige. "Dynamic synchronization between multiple cortical motor areas and muscle activity in phasic voluntary movements." *Journal of Neurophysiology* 84.5 (2000): 2622-2629.

Felleman, Daniel J., and DC Essen Van. "Distributed hierarchical processing in the primate cerebral cortex." *Cerebral cortex (New York, NY: 1991)* 1.1 (1991): 1-47.

Ferrell, W. R., S. C. Gandevia, and D. I. McCloskey. "The role of joint receptors in human kinaesthesia when intramuscular receptors cannot contribute." *The Journal of physiology* 386.1 (1987): 63-71.

Fogassi, Leonardo, et al. "Cortical mechanism for the visual guidance of hand grasping movements in the monkey: A reversible inactivation study." *Brain* 124.3 (2001): 571-586.

Gallese, Vittorio, et al. "Deficit of hand preshaping after muscimol injection in monkey parietal cortex." *Neuroreport: An International Journal for the Rapid Communication of Research in Neuroscience* (1994).

Georgopoulos, Apostolos P., et al. "On the relations between the direction of two-dimensional arm movements and cell discharge in primate motor cortex." *Journal of Neuroscience*2.11 (1982): 1527-1537.

Ghez, Claude, James Gordon, and MARIA FELICE Ghilardi. "Impairments of reaching movements in patients without proprioception. II. Effects of visual information on accuracy." *Journal of neurophysiology* 73.1 (1995): 361-372.

Godschalk, Moshe, et al. "Cortical afferents and efferents of monkey postarcuate area: an anatomical and electrophysiological study." *Experimental Brain Research* 56.3 (1984): 410-424.

Grafton, Scott T. "The cognitive neuroscience of prehension: recent developments." *Experimental brain research* 204.4 (2010): 475-491.

Graziano, Michael SA, Charlotte SR Taylor, and Tirin Moore. "Complex movements evoked by microstimulation of precentral cortex." *Neuron* 34.5 (2002): 841-851.

Guevara, Pamela, et al. "Robust clustering of massive tractography datasets." *Neuroimage* 54.3 (2011): 1975-1993.

Hatsopoulos, Nicholas G., and Aaron J. Suminski. "Sensing with the motor cortex." *Neuron* 72.3 (2011): 477-487.

Hatsopoulos, Nicholas G., and John P. Donoghue. "The science of neural interface systems." *Annual review of neuroscience* 32 (2009): 249-266.

Hatsopoulos, Nicholas G., Qingqing Xu, and Yali Amit. "Encoding of movement fragments in the motor cortex." *Journal of Neuroscience* 27.19 (2007): 5105-5114.

Heldstab, Sandra A., et al. "Manipulation complexity in primates coevolved with brain size and terrestriality." *Scientific reports* 6 (2016): 24528.

Herman, D., et al. "Responses of cat motor cortex neurons to cortico-cortical and somatosensory inputs." *Experimental brain research* 57.3 (1985): 598-604.

Hirsch, Judith A., José-Manuel Alonso, and R. Clay Reid. "Visually evoked calcium action potentials in cat striate cortex." *Nature* 378.6557 (1995): 612-616.

Hikosaka, Okihide, et al. "Deficits in manipulative behaviors induced by local injections of muscimol in the first somatosensory cortex of the conscious monkey." *Brain research* 325.1-2 (1985): 375-380.

Holtzman, Robert, ed. Surgery of the Diencephalon*. Springer Science & Business Media, 2012.*

Houk, James C., William Z. Rymer, and Patrick E. Crago. "Dependence of dynamic response of spindle receptors on muscle length and velocity." *Journal of Neurophysiology* 46.1 (1981): 143-166.

Houser, C. R., et al. "Morphological diversity of immunocytochemically identified GABA neurons in the monkey sensory-motor cortex." *Journal of neurocytology* 12.4 (1983): 617-638.

Iwamura, Yoshiaki. "Hierarchical somatosensory processing." *Current opinion in neurobiology* 8.4 (1998): 522-528.

Iriki, A. T. S. U. S. H. I., et al. "Long-term potentiation of thalamic input to the motor cortex induced by coactivation of thalamocortical and corticocortical afferents." *Journal of Neurophysiology* 65.6 (1991): 1435-1441.

Jackson, Andrew, Jaideep Mavoori, and Eberhard E. Fetz. "Long-term motor cortex plasticity induced by an electronic neural implant." *Nature* 444.7115 (2006): 56.

Jeannerod, Marc, et al. "Grasping objects: the cortical mechanisms of visuomotor transformation." *Trends in neurosciences* 18.7 (1995): 314-320.

Jia, Xiaoxuan, Seiji Tanabe, and Adam Kohn. "Gamma and the coordination of spiking activity in early visual cortex." *Neuron* 77.4 (2013): 762-774.

Jones, E. G., and T. P. S. Powell. "An anatomical study of converging sensory pathways within the cerebral cortex of the monkey." *Brain* 93.4 (1970): 793-820.

Jones, E. G., J. D. Coulter, and S. H. C. Hendry. "Intracortical connectivity of architectonic fields in the somatic sensory, motor and parietal cortex of monkeys." *Journal of Comparative Neurology* 181.2 (1978): 291-347.

Kaas, Jon H., Omar A. Gharbawie, and Iwona Stepniewska. "Cortical networks for ethologically relevant behaviors in primates." *American journal of primatology* 75.5 (2013): 407-414.

Kajikawa, Yoshinao, and Charles E. Schroeder. "How local is the local field potential?" *Neuron* 72.5 (2011): 847-858.

Kalaska, John F., et al. "A comparison of movement direction-related versus load direction-related activity in primate motor cortex, using a two-dimensional reaching task." *Journal of Neuroscience* 9.6 (1989): 2080-2102.

Kayser, Christoph, et al. "Spike-phase coding boosts and stabilizes information carried by spatial and temporal spike patterns." *Neuron* 61.4 (2009): 597-608.

Khawaja, Farhan A., James MG Tsui, and Christopher C. Pack. "Pattern motion selectivity of spiking outputs and local field potentials in macaque visual cortex." *Journal of Neuroscience* 29.43 (2009): 13702-13709.

Kinnischtzke, Amanda K., Erika E. Fanselow, and Daniel J. Simons. "Target-specific M1 inputs to infragranular S1 pyramidal neurons." *Journal of neurophysiology* 116.3 (2016): 1261-1274.

Klam, Francois, and Werner Graf. "Vestibular signals of posterior parietal cortex neurons during active and passive head movements in macaque monkeys." *Annals of the New York Academy of Sciences* 1004.1 (2003): 271-282.

Kraskov, Alexander, et al. "Ventral premotor–motor cortex interactions in the macaque monkey during grasp: response of single neurons to intracortical microstimulation." *Journal of Neuroscience* 31.24 (2011): 8812-8821.

Kropotov, Juri D. *Quantitative EEG, event-related potentials and neurotherapy*. Academic Press, 2010.

Krubitzer, Leah, et al. "Organization of area 3a in macaque monkeys: contributions to the cortical phenotype." *Journal of Comparative Neurology* 471.1 (2004): 97-111.

Kwan, H. C., et al. "Spatial organization of precentral cortex in awake primates. II. Motor outputs." *Journal of neurophysiology*41.5 (1978): 1120-1131.

Lansink, Carien S., et al. "Reward expectancy strengthens CA1 theta and beta band synchronization and hippocampal-ventral striatal coupling." *Journal of Neuroscience* 36.41 (2016): 10598-10610.

Lenz, F. A., et al. "Single unit analysis of the human ventral thalamic nuclear group." *Brain* 117.3 (1994): 531-543.

Lehmann, Sebastian J., and Hansjörg Scherberger. "Spatial representations in local field potential activity of primate anterior intraparietal cortex (AIP)." *PloS one* 10.11 (2015): e0142679.

Le Van Quyen, Michel, et al. "Comparison of Hilbert transform and wavelet methods for the analysis of neuronal synchrony." *Journal of neuroscience methods* 111.2 (2001): 83-98.

Lee, Han, et al. "Phase locking of single neuron activity to theta oscillations during working memory in monkey extrastriate visual cortex." *Neuron* 45.1 (2005): 147-156.

Li, Songting, et al. "The characterization of hippocampal theta-driving neurons—a time-delayed mutual information approach." *Scientific reports* 7.1 (2017): 5637.

Luppino, Giuseppe, et al. "Largely segregated parietofrontal connections linking rostral intraparietal cortex (areas AIP and VIP) and the ventral premotor cortex (areas F5 and F4)." *Experimental Brain Research* 128.1-2 (1999): 181-187.

Maunsell, J. H., and DAVID C. van Essen. "The connections of the middle temporal visual area (MT) and their relationship to a cortical hierarchy in the macaque monkey." *Journal of Neuroscience* 3.12 (1983): 2563-2586.

Mason, Carolyn R., et al. "Temporal profile of the directional tuning of the discharge of dorsal premotor cortical cells." *Neuroreport* 9.6 (1998): 989-995.

McGill, Kevin C., et al. "On the nature and elimination of stimulus artifact in nerve signals evoked and recorded using surface electrodes." *IEEE Transactions on Biomedical Engineering* 2 (1982): 129-137.

McILWAIN, JAMES T. "Retinotopic fidelity of striate cortex-superior colliculus interactions in the cat." *Journal of neurophysiology* 36.4 (1973): 702-710.

McIlwain, James T. "Topographic organization and convergence in corticotectal projections from areas 17, 18, and 19 in the cat." *Journal of neurophysiology* 40.2 (1977): 189-198.

Mitra, Partha. *Observed brain dynamics*. Oxford University Press, 2007.

Moran, Daniel W., and Andrew B. Schwartz. "Motor cortical representation of speed and direction during reaching." *Journal of neurophysiology* 82.5 (1999): 2676-2692.

Mori, Akio, Robert S. Waters, and Hiroshi Asanuma. "Physiological properties and patterns of projection in the cortico-cortical connections from the second somatosensory cortex to the motor cortex, area 4γ, in the cat." *Brain research*504.2 (1989): 206-210.

Mountcastle, Vernon B., et al. "Posterior parietal association cortex of the monkey: command functions for operations within extrapersonal space." *Journal of neurophysiology* 38.4 (1975): 871-908.

Mountcastle, Vernon B. *The sensory hand: neural mechanisms of somatic sensation*. Harvard University Press, 2005.

Muakkassa, Kamel F. "Frontal lobe inputs to primate motor cortex: evidence for four somatotopically organized'premotor'areas." *Brain Res.* 177 (1979): 176-182.

Murata, A. K. I. R. A., et al. "Parietal neurons related to memory-guided hand manipulation." *Journal of Neurophysiology* 75.5 (1996): 2180-2186.

Murata, Akira, et al. "Object representation in the ventral premotor cortex (area F5) of the monkey." *Journal of neurophysiology* 78.4 (1997): 2226-2230.

Murata, Akira, et al. "Selectivity for the shape, size, and orientation of objects for grasping in neurons of monkey parietal area AIP." *Journal of neurophysiology* 83.5 (2000): 2580-2601.

Nelson, R. J., et al. "Representations of the body surface in postcentral parietal cortex of Macaca fascicularis." *Journal of Comparative Neurology* 192.4 (1980): 611-643.

Nir, Yuval, et al. "Coupling between neuronal firing rate, gamma LFP, and BOLD fMRI is related to interneuronal correlations." *Current biology* 17.15 (2007): 1275-1285.

Nudo, Randolph J., et al. "Neurophysiological correlates of hand preference in primary motor cortex of adult squirrel monkeys." *Journal of Neuroscience* 12.8 (1992): 2918-2947.

Nudo, Randolph J., and Garrett W. Milliken. "Reorganization of movement representations in primary motor cortex following focal ischemic infarcts in adult squirrel monkeys." *Journal of neurophysiology* 75.5 (1996): 2144-2149.

O'Leary, John G., and Nicholas G. Hatsopoulos. "Early visuomotor representations revealed from evoked local field potentials in motor and premotor cortical areas." *Journal of neurophysiology* 96.3 (2006): 1492-1506.

Ohara, Shinji, et al. "Increased synchronization of cortical oscillatory activities between human supplementary motor and primary sensorimotor areas during voluntary movements." *Journal of Neuroscience* 21.23 (2001): 9377-9386.

Padberg, Jeffrey, et al. "Thalamocortical connections of parietal somatosensory cortical fields in macaque monkeys are highly divergent and convergent." *Cerebral Cortex* 19.9 (2009): 2038-2064.

Pandya, Deepak N., and Henricus GJM Kuypers. "Cortico-cortical connections in the rhesus monkey." *Brain research*13.1 (1969): 13-36.

Paninski, Liam. "Convergence properties of some spike-triggered analysis techniques." *NIPS*. 2002.

Paninski, Liam, et al. "Spatiotemporal tuning of motor cortical neurons for hand position and velocity." *Journal of neurophysiology* 91.1 (2004): 515-532.

Pardo-Vazquez, Jose L., et al. "Decision-making in the ventral premotor cortex harbinger of action." *Frontiers in integrative neuroscience* 5 (2011): 54.

Park, Michael C., et al. "Consistent features in the forelimb representation of primary motor cortex in rhesus macaques." *Journal of Neuroscience* 21.8 (2001): 2784-2792.

Pavlides, C. O. N. S. T. A. N. T. I. N. E., E. I. Z. O. Miyashita, and H. I. R. O. S. H. I. Asanuma. "Projection from the sensory to the motor cortex is important in learning motor skills in the monkey." *Journal of neurophysiology* 70.2 (1993): 733-741.

Peele, Talmage L. "Acute and chronic parietal lobe ablations in monkeys." *Journal of Neurophysiology* 7.5 (1944): 269-286.

Petrof, Iraklis, Angela N. Viaene, and S. Murray Sherman. "Properties of the primary somatosensory cortex projection to the primary motor cortex in the mouse." *Journal of neurophysiology* 113.7 (2015): 2400-2407.

Pillow, Jonathan W., et al. "Spatio-temporal correlations and visual signalling in a complete neuronal population." *Nature*454.7207 (2008): 995.

Poskanzer, Kira E., and Rafael Yuste. "Astrocytic regulation of cortical UP states." *Proceedings of the National Academy of Sciences* 108.45 (2011): 18453-18458.

Pruszynski, J. Andrew, et al. "Primary motor cortex underlies multi-joint integration for fast feedback control." *Nature* 478.7369 (2011): 387-390.

Quraishi, Salma, Barbara Heider, and Ralph M. Siegel. "Attentional modulation of receptive field structure in area 7a of the behaving monkey." *Cerebral Cortex* 17.8 (2006): 1841-1857.

Rajagovindan, Rajasimhan, and Mingzhou Ding. "Decomposing neural synchrony: toward an explanation for near-zero phase-lag in cortical oscillatory networks." *Plos one*3.11 (2008): e3649.

Rainer, Gregor. "Local field potential in the visual system." *Encyclopedia of Computational Neuroscience* (2015): 1534-1540.

Rathelot, Jean-Alban, and Peter L. Strick. "Subdivisions of primary motor cortex based on cortico-motoneuronal cells." *Proceedings of the National Academy of Sciences* (2009): pnas-0808362106.

Reimer, Jacob, and Nicholas G. Hatsopoulos. "Periodicity and evoked responses in motor cortex." *Journal of Neuroscience*30.34 (2010): 11506-11515.

Rieke, Fred, and David Warland. *Spikes: exploring the neural code*. MIT press, 1999.

Rizzolatti, Giacomo, et al. "Functional organization of inferior area 6 in the macaque monkey." *Experimental brain research*71.3 (1988): 491-507.

Rocco-Donovan, Mary, et al. "Characteristics of synaptic connections between rodent primary somatosensory and motor cortices." *Somatosensory & motor research* 28.3-4 (2011): 63-72.

Roe, A. W., and D. Y. Ts'o. "Functional connectivity between V1 and V2 in the primate." *Soc. Neurosci. Abstr*. Vol. 18. No. 11. 1992.

Romero, Maria C., and Peter Janssen. "Receptive field properties of neurons in the macaque anterior intraparietal area." *Journal of neurophysiology* 115.3 (2016): 1542-1555.

Rosen, I., and H. Asanuma. "Peripheral afferent inputs to the forelimb area of the monkey motor cortex: input-output relations." *Experimental brain research* 14.3 (1972): 257-273.

Rubino, Doug, Kay A. Robbins, and Nicholas G. Hatsopoulos. "Propagating waves mediate information transfer in the motor cortex." *Nature neuroscience* 9.12 (2006): 1549.

Sainburg, ROBERT L., et al. "Control of limb dynamics in normal subjects and patients without proprioception." *Journal of Neurophysiology* 73.2 (1995): 820-835.

Sakamoto, Takashi, Linda L. Porter, and Hiroshi Asanuma. "Long-lasting potentiation of synaptic potentials in the motor cortex produced by stimulation of the sensory cortex in the cat: a basis of motor learning." *Brain research* 413.2 (1987): 360-364.

Sakata, Hideo, et al. "Neural mechanisms of visual guidance of hand action in the parietal cortex of the monkey." *Cerebral Cortex* 5.5 (1995): 429-438.

Saleh, Maryam, et al. "Encoding of coordinated grasp trajectories in primary motor cortex." *The Journal of Neuroscience* 30.50 (2010): 17079-17090.

Saleh, Maryam, Kazutaka Takahashi, and Nicholas G. Hatsopoulos. "Encoding of coordinated reach and grasp trajectories in primary motor cortex." *Journal of Neuroscience*32.4 (2012): 1220-1232.

Saleh, Maryam, et al. "Fast and slow oscillations in human primary motor cortex predict oncoming behaviorally relevant cues." *Neuron* 65.4 (2010): 461-471.

Salin, P. A., et al. "Visuotopic organization of corticocortical connections in the visual system of the cat." *Journal of Comparative Neurology* 320.4 (1992): 415-434.

Sanes, Jerome N., et al. "Shared neural substrates controlling hand movements in human motor cortex." *Science* 268.5218 (1995): 1775-1777.

Sato, Takashi R., and Karel Svoboda. "The functional properties of barrel cortex neurons projecting to the primary motor cortex." *Journal of Neuroscience* 30.12 (2010): 4256-4260.

Schabrun, Siobhan M., Michael C. Ridding, and Timothy S. Miles. "Role of the primary motor and sensory cortex in precision grasping: a transcranial magnetic stimulation study." *European Journal of Neuroscience* 27.3 (2008): 750-756.

Schaffelhofer, Stefan, Andres Agudelo-Toro, and Hansjörg Scherberger. "Decoding a wide range of hand configurations from macaque motor, premotor, and parietal cortices." *Journal of Neuroscience* 35.3 (2015): 1068-1081.

Schieber, Marc H., and Lyndon S. Hibbard. "How somatotopic is the motor cortex hand area?." *Science* 261.5120 (1993): 489-492.

Schmidt, Mark, Glenn Fung, and Rmer Rosales. "Fast optimization methods for l1 regularization: A comparative study and two new approaches." *European Conference on Machine Learning*. Springer, Berlin, Heidelberg, 2007.

Seltzer, Benjamin, and Deepak N. Pandya. "Converging visual and somatic sensory cortical input to the intraparietal sulcus of the rhesus monkey." *Brain research* 192.2 (1980): 339-351.

Sergio, Lauren E., and John F. Kalaska. "Changes in the temporal pattern of primary motor cortex activity in a directional isometric force versus limb movement task." *Journal of neurophysiology* 80.3 (1998): 1577-1583.

Shinoura, Nobusada, et al. "Fibers connecting the primary motor and sensory areas play a role in grasp stability of the hand." *Neuroimage* 25.3 (2005): 936-941.

Siegelbaum, Steven A., and A. J. Hudspeth. *Principles of neural science*. Eds. Eric R. Kandel, James H. Schwartz, and Thomas M. Jessell. Vol. 4. New York: McGraw-hill, 2000.

Silva, Laurie R., Yael Amitai, and Barry W. Connors. "Intrinsic oscillations of neocortex generated by layer 5 pyramidal neurons." *Science* 251.4992 (1991): 432.

Snyder, Lawrence H., Aaron P. Batista, and Richard A. Andersen. "Coding of intention in the posterior parietal cortex." *Nature* 386.6621 (1997): 167.

Stark, Eran, et al. "Distinct movement parameters are represented by different neurons in the motor cortex." *European Journal of Neuroscience* 26.4 (2007): 1055-1066.

Stepniewska, Iwona, Todd M. Preuss, and Jon H. Kaas. "Architectionis, somatotopic organization, and ipsilateral cortical connections of the primary motor area (M1) of owl monkeys." *Journal of Comparative Neurology* 330.2 (1993): 238-271.

Sur, Mriganka, Preston E. Garraghty, and Charles J. Bruce. "Somatosensory cortex in macaque monkeys: laminar differences in receptive field size in areas 3b and 1." *Brain research* 342.2 (1985): 391-395.

Taira, M., et al. "Parietal cortex neurons of the monkey related to the visual guidance of hand movement." *Experimental brain research* 83.1 (1990): 29-36.

Taira, Masato, et al. "On the relations between single cell activity in the motor cortex and the direction and magnitude of three-dimensional static isometric force." *Experimental brain research* 109.3 (1996): 367-376.

Takahashi, Kazutaka, et al. "Encoding of both reaching and grasping kinematics in dorsal and ventral premotor cortices." *Journal of Neuroscience* (2017): 1537-16.

Takahashi, Kazutaka, et al. "Large-scale spatiotemporal spike patterning consistent with wave propagation in motor cortex." *Nature communications* 6 (2015): 7169.

Takahashi, Kazutaka, et al. "Propagating waves in human motor cortex." *Frontiers in human neuroscience* 5 (2011): 40.

Tanaka, K. E. I. J. I. "Cross-correlation analysis of geniculostriate neuronal relationships in cats." *Journal of neurophysiology* 49.6 (1983): 1303-1318.

Thomas Jessell, Steven Siegelbaum, and A. J. Hudspeth. *Principles of neural science*. Eds. Eric R. Kandel, James H. Schwartz, and Thomas M. Jessell. Vol. 4. New York: McGraw-hill, 2000.

Thompson, We D., S. D. Stoney Jr, and H. Asanuma. "Characteristics of projections from primary sensory cortex to motorsensory cortex in cats." *Brain research* 22.1 (1970): 15-27.

Traub, Roger D., et al. "Cellular mechanisms of neuronal population oscillations in the hippocampus in vitro." *Annu. Rev. Neurosci.* 27 (2004): 247-278.

Ungerleider, Leslie G., and Robert Desimone. "Cortical connections of visual area MT in the macaque." *Journal of Comparative Neurology* 248.2 (1986): 190-222

van Wingerden, Marijn, et al. "Theta-band phase locking of orbitofrontal neurons during reward expectancy." *Journal of Neuroscience* 30.20 (2010): 7078-7087.

Wolpaw, Jonathan R. "Electromagnetic muscle stretch strongly excites sensorimotor cortex neurons in behaving primates." *Science* 203.4379 (1979): 465-467.

Zarzecki, P., Y. Shinoda, and H. Asanuma. "Projection from area 3a to the motor cortex by neurons activated from group I muscle afferents." *Experimental brain research* 33.2 (1978): 269-282.